Universitetet i Stavanger

DET TEKNISK-NATURVITENSKAPELIGE FAKULTET

MASTEROPPGAVE

Studieprogram/spesialisering: Master i realfag med teknologi	Vår semesteret, 2009 Åpen
Forfatter: Siv Gjertrud Evje	…… (signatur forfatter)
Faglig ansvarlig: Svein Magne Skjaeveland Veiledere: Svein Magne Skjaeveland Johan Olav Helland	
Tittel på oppgaven: Validation of a capillary pressure correlation for dynamic wettability alteration	
Studiepoeng: 30	
Emneord: wettability, contact angle, capillary pressure, saturation, drainage, imbibition, correlation, Cassie's law	Sidetall: 47 Stavanger, 15.06.2009.

VALIDATION OF A CAPILLARY PRESSURE CORRELATION FOR DYNAMIC WETTABILITY ALTERATION

SIV GJERTRUD EVJE

ABSTRACT. The purpose of this thesis is to try to evaluate a capillary pressure correlation $P_c(S_w, \theta)$ that previously has been proposed, by using a pore model. The correlation depends on the water saturation S_w and an averaged contact angle θ representing the wetting state of the porous media in question. In particular, there are four free parameters that must be specified.

Necessary details concerning the pore model and how it is used to describe primary drainage and imbibition are included. Capillary pressure curves are generated by the pore model by increasing (drainage) or decreasing (imbibition) the capillary pressure respectively, while the corresponding water saturation of the porous media is obtained through a series of calculations. This is done by consecutively evaluation of the fluid configurations of the pores in the model, which in turn depend on the corresponding capillary entry pressures. A presentation of the MS-P method used in the calculations of the capillary entry pressures is also included.

We restrict the evaluation of the capillary pressure correlation to an imbibition process where the pore model relies on a distribution of local contact angles θ_a. In order to compare the correlation $P_c(S_w, \theta)$ with capillary pressure curves generated by the pore model, a relation between the averaged contact angle θ and the distribution of local contact angles θ_a, must be specified. We consider two choices. First, a direct relation where $\theta = \theta_a$, and then a relation based on Cassie's law. A rather general framework for construction of θ_a and θ such that Cassie's law is obeyed, is proposed. For the evaluation we use an optimization algorithm where we identify the four unknown parameters which give a best fit. These calculations show that it is possible to obtain a good match when Cassie's law is taken into account. In particular, it is likely that even better results can be obtained by refining the construction of the distribution θ_a, relying on the suggested approach.

Key words. wettability, contact angle, capillary pressure, saturation, drainage, imbibition, correlation, Cassie's law

Date: June 15, 2009.

Contents

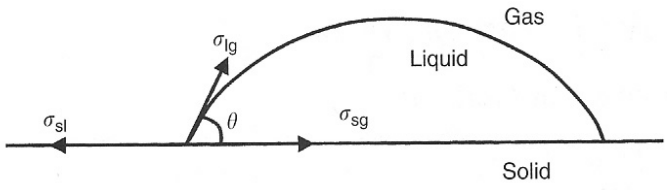

FIGURE 1. Contact angle of a liquid on a solid surface.

1. INTRODUCTION

In this section we first introduce and describe some concepts and quantities that are essential for the understanding of the investigations of this thesis. Then a presentation of the main objectives of this work is given.

1.1. **Some definitions.**

Wettability. When immiscible fluids are present simultaneously in a porous media they compete for the occupancy of the pore surface. *Wettability* can be defined as the tendency of one of the fluids to spread on or adhere to the solid surface [13]. In an oil-water situation in a porous media, it is a measure of the preference that the solid surface has for either oil or water. According to [8] and references therein, a system may be characterized as *mixed-wet*. For a reservoir rock originally strongly water-wet, this is a description indicating that invasion of oil into the reservoir has resulted in a change of wettability (to oil-wet) in parts of the rock surface while other parts remain water-wet. In this study we consider mixed wettability at the pore level where invasion of oil into strongly water-wet angular pores leaves the corners water-wet while a part of the walls of the pores are wettability-altered. The wettability of a porous media system is important because it is a major factor controlling the location, flow and distribution of the present fluids. The wettability will therefore influence different analysis including capillary pressure, relative permeability and water flood behavior, etc.

Contact angle. Contact angle is a quantitative measure of the wetting of a solid by a liquid. It is the angle formed by the three phase boundary where a liquid, gas (or a second immiscible liquid) and solid intersect. The three phases are denoted by l, g and s, respectively. The force balance at the point on the three-phase line of contact along the liquid-gas/liquid-solid boundary is expressed by Young's equation developed in 1805, [1]:

$$\sigma_{lg} \cos\theta_{lg} = \sigma_{sg} - \sigma_{sl} \tag{1}$$

where σ_{lg}, σ_{sg} and σ_{sl} are the interfacial tensions between the phases in contact, and θ_{lg} is the liquid-gas/liquid contact angle. It represents the state of the drop which has the minimal Gibb's energy. The contact angle of a gas-liquid-solid or a liquid-liquid-solid system may have any value between 0° and 180°. It is customary to classify the fluids into two categories: wetting and non-wetting fluid. For wetting fluids, $0° \leq \theta < 90°$, and for

non-wetting fluids, $90^\circ < \theta \leq 180^\circ$. We distinguish between the *advancing* and *receding* contact angle, which will be denoted by θ_a and θ_r respectively. If the drop volume (of the liquid in Fig. 1) is increased, the contact line appears to be pinned, while the contact angle increases. The contact angle eventually reaches a maximum value called the advancing contact angle which is the largest possible angle reached before the contact line expand. Similar phenomena occurs when the drop volume is decreased. The smallest possible contact angle reached before the contact line decreases is called the receding contact angle. The observed contact angle thus depends on the way the system is prepared. The relevant contact angle throughout this study is the oil-water contact angle (measured through the water phase) at the boundary between the two phases oil and water at the wall of a capillary. In the following we shall study two-phase fluid displacements in a pore-scale network where the contact angle is determined by the direction of the displacement. The difference between the advancing and receding contact angle, $\theta_a - \theta_r$, what we call the *contact angle hysteresis*, is mainly due to surface roughness and surface heterogeneity. Other factors can be liquid absorption and/or retention (swelling) and the formation of a liquid film left behind a fluid drop during the contact line retracting [10].

Capillary pressure. An important parameter in the study of a porous medium containing two or more immiscible fluids is the capillary pressure. This is because the capillary forces (together with viscous and gravitational forces) control the distribution and the flow of the immiscible phases. In porous media, immiscible fluids are separated from each others by curved interfaces, across which there exists a pressure difference called the capillary pressure, Pc. As the capillary pressure is a result of the interfacial tension and the curvature (and hence the contact angle) of the immiscible fluids present, it is dependent on the wetting state of the porous media. Pc is generally defined as the pressure difference between the non-wetting phase and the wetting phase, that is

$$Pc = P_{nonwetting} - P_{wetting}. \tag{2}$$

In the following study of two-phase fluid flow (oil-water) in porous media, the capillary pressure is given by

$$Pc = P_{oil} - P_{water}. \tag{3}$$

Saturation. In two-phase oil-water fluid flow the capillary pressure curves are described in terms of S_w, where S_w is the water-saturation. We also recall the fundamental relations $S_w + S_o = 1$, where S_o is the oil-saturation. S_{wr} is the residual or irreducible water saturation and S_{or} is the residual or irreducible oil saturation.

Drainage. Drainage, or dewetting, is the process where a non-wetting phase displaces a wetting phase. Normally, drainage is referred to as the process where oil displaces water in the pores of a porous media, i.e the water saturation S_w is decreasing. *Primary drainage* is thus the first time oil invades originally water-filled, strongly water-wet pores, and starts from $S_w = 1$. To initiate the drainage of a pore system a threshold capillary pressure has to be overcome. This threshold pressure corresponds to the *capillary entry pressure* for the pores that have the pore throats with largest radius. If the pressure of the oil-phase

is increased, smaller pores will be invaded, leading to a decreasing S_w. Continuing this process, an irreducible water-saturation S_{wr} will be approached. At this point, no further invasion of oil is possible. After an imbibition process (see below), *secondary drainage* starts from an irreducible oil-saturation, $S_o = S_{or}$, and approaches S_{wr} as the capillary pressure of the oil is increased. Spontaneous (secondary) drainage occurs for negative capillary pressure, and forced (secondary) drainage for positive capillary pressure. Primary and secondary drainage curves with the asymptotes at S_{wr} and S_{or} are illustrated in Fig. 11.

Imbibition. Imbibition, or dewetting, is the process where the wetting phase displaces the non-wetting phase. Here it is referred to as the process where water displaces oil, i.e. the water saturation S_w is increasing. *Primary imbibition* starts from $S_o = 1$ and *secondary imbibition* from $S_w = S_{wr}$. Spontaneous imbibition occurs for positive capillary pressure and forced imbibition for negative capillary pressure. Imbibition curves are shown in Fig. 11. The difference of the secondary drainage and imbibition curves is due to the contact angle hysteresis mentioned above. The receding contact angle is relevant in the drainage process and the advancing contact angle in the imbibition process. In this study we will concentrate on the secondary imbibition process. After the pores have been invaded by oil through primary drainage, the porous media is allowed to (first spontaneous and then forced) imbibe water and S_w is increased starting from S_{wr} until an irreducible oil-saturation is reached, that is when $S_w = 1 - S_{or}$. Invasion of water may results in changes of the configuration of the pores which occurs at certain levels of the capillary pressure called capillary entry pressures.

1.2. **Objectives.** After this introduction of basic concepts and ideas, we now state what will be the main objective of this work.

By using a pore model we shall try to evaluate a capillary pressure correlation $P_c(S_w, \theta)$ that previously has been proposed [12], which depends on the water saturation S_w and an averaged contact angle θ representing the wetting state of the porous media in question. In particular, there are four free parameters that must be specified. We restrict the evaluation to an imbibition process where the pore model relies on a distribution of local contact angles θ_a. In order to compare the correlation with capillary pressure curves generated by the pore model, a relation between the averaged contact angle θ and the distribution of local contact angles θ_a must be specified. We consider two choices. First, a direct relation where $\theta = \theta_a$, and then a relation based on Cassie's law. For the evaluation we use an optimization algorithm where we identify the four unknown parameters which gives a best fit.

The investigations are structured as follows:

(1) Firstly, we shall describe some of the details of the pore model, i.e., the pore geometry, the primary drainage, and imbibition processes (Section 2.1).
(2) Secondly, the Mayer, Stowe and Princen (MS-P) method for calculating the capillary entry pressures is presented. This method is a central ingredient and is repeatedly used in the simulations done by the pore model (Section 2.2).

(3) Thirdly, we introduce the capillary pressure correlation (Section 3).
(4) Equipped with the pore model, we try to validate the capillary pressure correlation. As a first approach, a straight forward way of relating an averaged contact angle θ to wetting states in the pore model is suggested (Case I) (Section 4.1). Then Cassie's law is described and applied in the correlation to connect θ and θ_a (Case II) (Section 4.3).
(5) Finally, some concluding remarks are made (Section 5).

2. A pore scale model

2.1. **Derivation of the pore scale model.** In this section we describe the pore model used in this study as presented in [4] and [6]. We will start by describing the geometry of the pores and then give a presentation of the processes involved. The model assumes a bundle of tubes representing the pore network. The cross-sections of the tubes have the shape of regular stars with three corners which include an equilateral triangle. The developed Matlab code for the model generates 2-phase capillary pressure- and relative permeability curves for primary drainage with wettability alteration, imbibition and secondary drainage with hysteresis loops. We will concentrate on the processes of *primary drainage* and *imbibition* and the corresponding capillary pressure curves.

The geometry of the pores in the model. The geometry of a regular star-shaped pore is described by the radii R of the inscribed circle, the number of corners n in each pore and the half angle α of the corners in the pore [6]. In the pore model, the pore sizes, quantified by the radii R, are supposed to be determined from a distribution function. In the work of Helland the pore-size frequency is described by a truncated two-parameter Weibull distribution [8]. This is a flexible distribution that often has been employed for this purpose [7]. The pore sizes R are then selected from the cumulative distribution function in the following manner: Pick random numbers $\mathrm{x} \in [0,1]$ and calculate the inscribed radius from

$$R = R_{\mathrm{ch}}\Big(-\ln[(1-\mathrm{x})\exp(-\Big[\frac{R_{\max}-R_{\min}}{R_{\mathrm{ch}}}\Big]^{\eta}) + \mathrm{x}]\Big)^{\frac{1}{\eta}} + R_{\min}. \tag{4}$$

where $R_{\max}$, $R_{\min}$ and R_{ch} are the inscribed radii of the largest, smallest and the characteristic pore sizes, respectively, and η is a dimensionless parameter. Other distributions, like the log-normal- and beta-distributions, could also be used in the pore model to determine a realistic distribution of the pore-sizes. For simplicity, however, we let R take a uniform distribution with the density function

$$\begin{aligned} f(R) &= \frac{1}{R_{\max}-R_{\min}}, \qquad && R_{\min} < R \le R_{\max} \\ &= 0, && \text{elsewhere.} \end{aligned} \tag{5}$$

The half angles of the corners of a star-shaped pore, α, must satisfy

$$0 < \alpha \le \alpha_{\max}, \qquad \text{where} \qquad \alpha_{\max} = \frac{\pi}{2} - \frac{\pi}{n}, \tag{6}$$

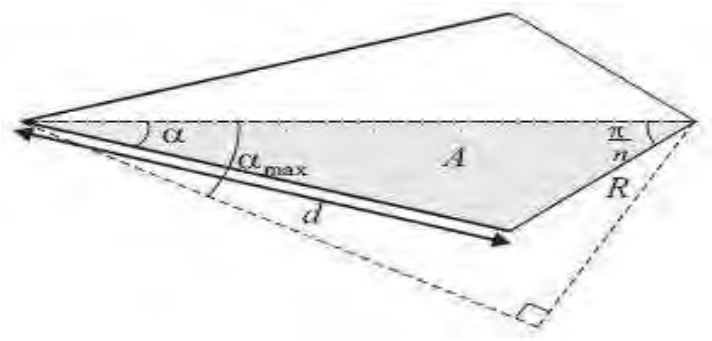

FIGURE 2. The cross-section of a corner of a n-cornered star-shaped tube. The shaded area corresponds to $1/2n$ of the total cross-section. The dashed lines shows the geometry for the limiting case $\alpha = \alpha_{\max}$, [4].

where n is the number of corners in the pore. The limiting case, $\alpha = \alpha_{\max}$, for stars with three corners corresponds to the case of an equilateral triangle, i.e. $\alpha_{\max} = \frac{\pi}{6}$. In the pore model we have assumed a linear relationship between the half angle of the corners of the pores and the inscribed radius R. This is given by

$$\alpha(R) = aR + b, \quad \text{where} \quad a = \frac{\alpha_{\min} - \alpha_{\max}}{R_{\max} - R_{\min}}, \quad b = \alpha_{\max} - \Big(\frac{\alpha_{\min} - \alpha_{\max}}{R_{\max} - R_{\min}}\Big) R_{\min}, \tag{7}$$

for $R \in [R_{\min}, R_{\max}]$.

Other relationships could also be chosen, and the parameters may be varied independently.

The cross-sectional area of a star-shaped tube is related to the inscribed radius R and the half angle of the corners α as shown below in Eq. (8) [6]. Since the corners of a regular star is symmetric, we can make our calculations concerning the cross-sections by considering just one half of a corner of the pore, see Fig. 2. The shaded area A in the figure is given by

$$A = \frac{R^2}{2} \frac{\sin(\alpha + \frac{\pi}{n}) \sin\frac{\pi}{n}}{\sin\alpha}, \tag{8}$$

and represents $\frac{1}{2n}$ of the entire pore cross-section. The distance d is given by

$$d = \frac{R \sin\frac{\pi}{n}}{\sin\alpha}. \tag{9}$$

The total area and perimeter of the entire pore cross-section are therefore

$$A_p = 2nA \qquad \text{and} \qquad d_p = 2nd, \tag{10}$$

respectively. In the model used throughout this work, however, we just consider pores with three corners i.e. $n = 3$.

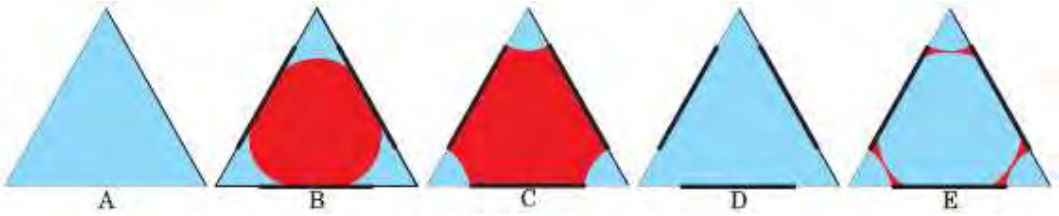

FIGURE 3. The possible fluid configurations of the pores during primary drainage and imbibition [4].

Primary drainage. Initially all the tubes are filled with water and are strongly water-wet as illustrated in configuration A of Fig. 3 for a tube with the form of an equilateral triangle.

The primary drainage process is simulated by stepwise increasing the capillary pressure $Pc = p_o - p_w$ until a maximum value $Pc^{\max}$ is reached. Oil invades a tube when the capillary pressure is increased to the capillary entry pressure for the tube. The capillary entry pressure depends on the geometry and wettability of the tube and is calculated by the Mayer-Stowe-Princen (MS-P) method described in Section 2.2.

During primary drainage, the (receding) contact angle denoted by θ_{pd} is small. Oil invasion may result in two different situations depending on the size of θ_{pd}.

If $\theta_{pd} < \pi/2 - \alpha$, the tubes are supposed to reach the fluid configuration shown in Fig. 4 for an equilateral triangle where oil has occupied the bulk area of the tube while the corners are still waterfilled. It is assumed that the invading oil immediately contacts the pore walls, i.e. a possible waterfilm between the oil and the pore walls is neglected. The wettability of the sides of the pores are then altered while the corners are still water-wet. The wettability altered part of the pore walls is demonstrated in Fig. 4 by the bold lines along the sides.

To construct the capillary pressure curve $Pc(S_w, \theta_{pd})$ we need to find the total water-saturation S_w of the porous medium for each pressure step. At every step $\triangle P$ during primary drainage all the tubes are therefore tested for invasion by comparing the present level of the capillary pressure with the entry pressures for the tubes. The fluid configurations are updated and the water content of each tube is calculated. The existing capillary pressure may be expressed by the Young-Laplace equation [3]

$$Pc = \sigma\Big(\frac{1}{R_1} + \frac{1}{R_2}\Big) \tag{11}$$

where σ is the interfacial tension between the two phases and R_1 and R_2 are the principal radii of curvature for the interface separating the phases. The tubes considered are supposed to have a constant cross-section along the length of the tubes and the capillary pressure with $R_1 = \infty$ and $R_2 = r_{ow}$ is therefore given by

$$Pc_{ow} = \frac{\sigma_{ow}}{r_{ow}}. \tag{12}$$

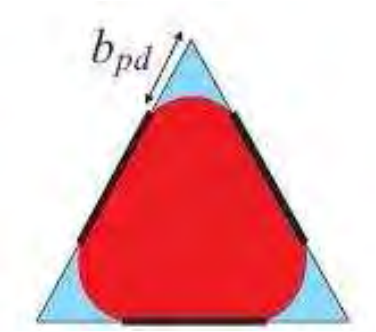

FIGURE 4. The fluid configuration of the tubes that has been invaded by oil during primary drainage (water in blue color and oil in red color). The bold lines along the sides indicate altered wettability.

In Eq. (12), r_{ow} is the radius of the cross-sectional circular arc of interface, denoted by the *arc meniscus* (AM), separating the bulk fluid (here oil) and the fluid in a corner (here water), see Fig. 9. If oil has invaded a tube, the total area of the corners occupied by water is

$$A_w(\theta) = 3r_{ow}^2\Big(\theta_{pd} + \alpha - \frac{\pi}{2} + \cos\theta_{pd}\Big(\frac{\cos\theta_{pd}}{\tan\alpha} - \sin\theta_{pd}\Big)\Big). \tag{13}$$

At every higher level of pressure the value of r_{ow} changes (decreases), and so also the area $A_w(\theta)$ as the oil is squeezed into the corners of the tubes. At the same time the oil will constantly enter smaller tubes. For the tubes not yet invaded by oil the relevant area is of course

$$A_w(\theta) = A_p, \tag{14}$$

where A_p is the total area of cross-section of the tube given by Eq.(10).

The values of $A_w(\theta)$ and A_p are then used in the calculations of the corresponding water saturation for the whole bundle of tubes needed to generate the capillary pressure curve for primary drainage. This is done for every step in Pc as long as the capillary pressure does not exceed the maximum value $Pc^{\max}$. The process will also terminate if the water-saturation is less than a given value. For each pressure step, the total water-saturation is

$$S_w^{pd} = \frac{\Sigma_{i=1}^N A_{w,i}}{\Sigma_{i=1}^N A_{p_i}}, \tag{15}$$

where N denotes the number of tubes. This also gives the corresponding oil-saturation S_o as

$$S_o^{pd} = 1 - S_w^{pd}. \tag{16}$$

The minimum radius of r_{ow} for a pore during primary drainage is given by (12) as

$$r_{ow}^{\min} = \frac{\sigma_{ow}}{Pc^{\max}}, \tag{17}$$

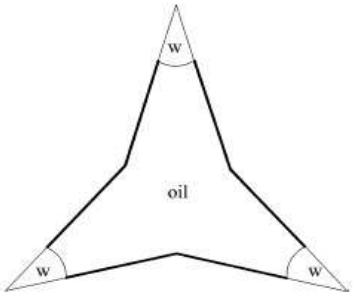

FIGURE 5. Illustration of configuration C for a star-shaped pore, [2].

and represents the curvature of the AM's at the end of primary drainage. The distance b_{pd} in the corners, see Fig. 4, that remains water-wet is at this point given by

$$b_{pd} = \frac{\sigma_{ow}\cos\left(\theta_{pd}+\alpha\right)}{Pc^{\max}\sin\alpha}. \tag{18}$$

If we have the situation with a larger contact angle i.e. $\theta_{pd} \geq \pi/2 - \alpha$, the invading oil will fill the cross-section of the pores completely.

Imbibition. In the imbibition process the pores are filled during water-flooding mainly by the mechanism of piston-like displacement [8]. Imbibition is simulated by decreasing the capillary pressure stepwise starting from the final point of primary drainage. For the pores which have reached the configuration in Fig. 4 during primary drainage, a change of configuration now depends on the change of wettability in the pore represented by the contact angle, which influence the capillary entry pressure, [2, 4]. From being strongly water-wet with the small receding contact angle $\theta_r = \theta_{pd}$, the pores are now mixed-wet with the advancing contact angle $\theta_a \geq \theta_{pd}$ defined on the area of the pore walls with altered wettability. As the capillary pressure is decreased and water is allowed to invade, any movement on the wettability altered surface occurs at the (increased) advancing contact angle θ_a. The position where an AM contacts the pore wall is now temporarily fixed at the distance b_{pd} from the corner due to the difference between θ_r and θ_a, but the curvature changes. The AM's are now hinging with the hinging contact angle θ_h, increasing from θ_{pd} to θ_a, see configuration C in Fig. 3 and Fig. 5. From Eq. (18) we may express the contact angle θ_{pd} as

$$\theta_{pd} = \cos^{-1}\Big[\frac{Pc^{\max}\ b_{pd}\ \sin\alpha}{\sigma_{ow}}\Big] - \alpha. \tag{19}$$

and the hinging contact angle is thus given by

$$\theta_h = \cos^{-1}\Big[\frac{Pc\ b_{pd}\ \sin\alpha}{\sigma_{ow}}\Big] - \alpha. \tag{20}$$

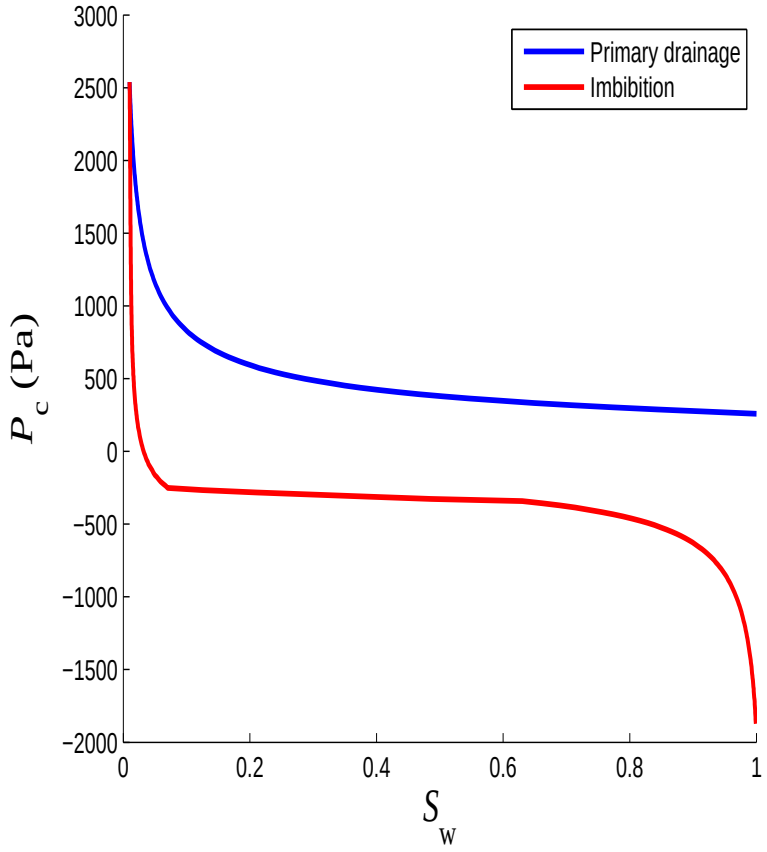

FIGURE 6. Primary drainage and imbibition curves generated by the pore model when the contact angle, $\theta_a(R)$, varies linearly with the size of the pores.

A change of the fluid configuration for a tube now occurs when the capillary pressure is lowered to the corresponding capillary entry pressure. The following displacements from configuration C are possible during imbibition, and the most favorable, depending on Pc, occurs [4]:

(1) For $\theta_a < \frac{\pi}{2} - \alpha$: $C \rightarrow B \rightarrow D$ or $C \rightarrow D$.
(2) For $\frac{\pi}{2} - \alpha \leq \theta_a \leq \frac{\pi}{2} + \alpha$: $C \rightarrow D$.
(3) For $\theta_a > \frac{\pi}{2} + \alpha$: $C \rightarrow D$ or $C \rightarrow E \rightarrow D$.

We note that configuration C is the same as the configuration in Fig. 4, but now illustrated with a negative capillary pressure. The possible fluid configurations the pores can obtain during imbibition are shown in Fig. 3. The capillary entry pressures required for the different displacements are described in the next section. As for primary drainage all the tubes are continuously tested for their present conditions at every step in Pc. The

water contents are thus calculated to decide the actual water-saturation of the sample corresponding to the present capillary pressure.

The relation between θ_a and the inscribed radius R for the different pores in the model should be determined by a distribution function $\theta_a(R)$ that gives a realistic relation between the contact angle and the pore-sizes.

To sum up: For a given $\theta_a(R)$, representing a certain wetting state, we can use the pore model to obtain a corresponding capillary pressure curve $Pc^{Pore}(S_w)$. We may use the following notation:

$$\theta_a(R) \overset{\text{Pore model}}{\longrightarrow} Pc^{Pore}(S_w). \tag{21}$$

First, we assume a wetting state where $\theta_a(R)$ depends linearly on R as follows

$$\theta_a^1(R) = aR + b, \quad \text{where} \quad a = \frac{\theta_{a_{\max}} - \theta_{a_{\min}}}{R_{\max} - R_{\min}}, \quad b = \theta_{a_{\min}} - \Big(\frac{\theta_{a_{\max}} - \theta_{a_{\min}}}{R_{\max} - R_{\min}}\Big) R_{\min}, \tag{22}$$

for $R \in [R_{\min}, R_{\max}]$. As a second example we assume that

$$\theta_a^2(R) = \theta_a^* \quad \text{(constant)}, \tag{23}$$

for $R \in [R_{\min}, R_{\max}]$ and $\theta_a^* \in [\theta_{a_{\min}}, \theta_{a_{\max}}]$. Below, the two different ways of assigning a distribution for the advancing contact angle are explored.

Examples of curves generated by the pore model. We have generated primary drainage and imbibition curves by using the pore model with $N = 300$ tubes.

The pore-sizes are determined from the uniform distribution

$$\begin{aligned} &\{R_i\}_{i=1}^N \ \text{where} \ R_1 = R_{\min}, \qquad R_i = R_{\min} + (i-1)\triangle R, \qquad i = 2, ..., N-1 \\ &\qquad\qquad \text{and} \ R_N = R_{\max}. \end{aligned} \tag{24}$$

Here $R_{\min} = 10\mu m$ represents the smallest pore size and $R_{\max} = 100\mu m$ represents the largest. Moreover $\triangle R = (R_{\max} - R_{\min})/(N-1)$.

With the linear relationship we have chosen for $\alpha(R)$ as given by (7), α takes the following values

$$\begin{aligned} &\{\alpha_i\}_{i=1}^N \ \text{where} \ \alpha_1 = \alpha_{\max}, \qquad \alpha_i = \alpha_{\max} + (i-1)\triangle\alpha, \qquad i = 2, ..., N-1 \\ &\qquad\qquad \text{and} \ \alpha_N = \alpha_{\min}. \end{aligned} \tag{25}$$

The smallest angle is $\alpha_{\min} = \pi/180 = 1^\circ$, the largest $\alpha_{\max} = \pi/6 = 30^\circ$ and we have $\triangle\alpha = (\alpha_{\min} - \alpha_{\max})/(N-1)$.

All the simulations are made with $\theta_{pd} = 0^\circ$, the oil-water interfacial tension $\sigma_{ow} = 0.020N/m$, the pressure step $\triangle Pc = 15$Pa and the value of Pc at the end of primary drainage $Pc^{\max} = 10000$Pa.

In the first example, we use the linear function for $\theta_a(R)$ as given by Eq.(22). With this choice, $\theta_a(R)$, which must satisfy $\theta_a \geq \theta_{pd}$, is in the range

$$\begin{aligned} &\{\theta_a\}_{i=1}^N \ \text{where} \ \theta_{a_1} = \theta_{a_{\min}}, \qquad \theta_{a_i} = \theta_{a_{\min}} + (i-1)\triangle\theta_a, \qquad i = 2, ..., N-1 \\ &\qquad\qquad \text{and} \ \theta_{a_N} = \theta_{a_{\max}}, \end{aligned} \tag{26}$$

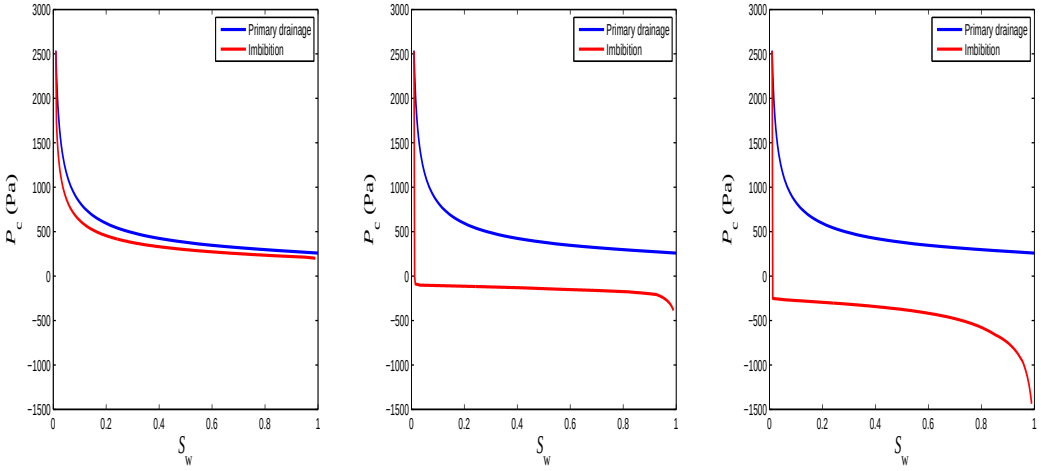

FIGURE 7. Examples of imbibition curves generated by the pore model with constant contact angles, θ_a^*, for all the pores. **Left:** $\theta_a^* = 40°$. **Middle:** $\theta_a^* = 110°$. **Right:** $\theta_a^* = 180°$. For comparison, the primary drainage curve has also been included.

where we let $\theta_{a_{\min}} = 40°$, $\theta_{a_{\max}} = 180°$ and $\triangle\theta_a = (\theta_{a_{\max}} - \theta_{a_{\min}})/(N-1)$. Fig. 6 illustrates the generated curves obtained for this example.

In the next example a constant contact angle is assumed for all the tubes during imbibition as described by Eq. (23). Fig. 7 shows three different imbibition curves which are generated with a constant contact angle for all the tubes. The curves are made for $\theta_a = 40°$, $\theta_a = 110°$ and $\theta_a = 180°$.

We observe that the main difference between using a linear relation (22) and the constant relation (23) is the behavior in the neighborhood of the endpoints.

2.2. **The MS-P method.** The fluid displacements during primary drainage (oil displaces water) and imbibition (water displaces oil) occur in general by the mechanism of piston-like invasion [8]. The invading fluid enters the pore from one of the ends. For a given pore, a fluid is able to invade when the capillary pressure reaches the capillary entry pressure required for the displacement. The capillary entry pressure is determined by the pore size, pore shape and the local contact angle representing the wettability of the given pore. In the case where pores are modeled as straight tubes of circular cross-sections, a given cross-section can be filled by only one phase. The capillary entry pressure for displacements in these pores are described by the Young-Laplace equation given by Eq (12). However, when noncircular cross-sections are assumed, a given cross-section may be filled by more than one phase. In angular pores oil may be present in the centre of the cross-section, while water wetting layers occupy the corners. The calculation of the capillary entry pressures for fluid-displacements in this case are more complicated. In this section we shall use the (MS-P) method developed by Mayer, Stowe and Princen to derive the capillary entry pressure for piston-like invasion into uniformly wetted, regular, n-sided pores. The presentation of

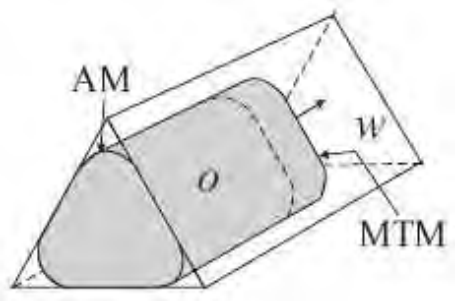

FIGURE 8. Piston-like invasion of oil into a waterfilled tube. In the derivation of the capillary entry pressure we consider a small displacement of the MTM along the tube length.

this method follows the approach of Helland [8] and [4], and gives the expressions for the capillary entry pressure relevant for two-phase flow in regular star-shaped pores.

In the following we first consider the invasion of oil into a water-wet tube completely filled with water i.e. for primary drainage. As mentioned in Section 2.1 this may result in two different configurations, depending on the value of the contact angle. At the end of the section we briefly present the expressions for capillary entry pressure for the possible fluid displacements during imbibition.

Case (1): If $\theta_{ow} < \frac{\pi}{2} - \alpha$, the invasion of oil results in the configuration shown in Fig. 4 for an equilateral triangle. In this case the cross-section of the tube obtain a configuration where the oil occupies the bulk area and the corners are still filled with water. The invading interface separating the bulk fluids along the tube is called the *main terminal meniscus* (MTM). The *arc meniscus* (AM) is the interface separating the oil in the bulk and the water in the corners of the tube, see Fig. 8. The MS-P method assumes that capillary pressure is uniform, and thus the effect of gravity on the shape of the interface is neglected, as is also the contact angle hysteresis.

Since the cross-sectional shape is assumed to be constant along the tube, the MTM is supposed to pass through the entire tube length at the capillary entry pressure. The curvature of the AM's are therefore constant along the tube and equal to the entry curvature of the MTM during the displacement. The capillary entry pressure is therefore given by Eq. (12) where r_{ow} is the entry radius of curvature of the AM's sufficiently far behind the MTM measured through the oil phase. The MS-P method is founded on an energy balance equation which equates the virtual work with the associated change of surface free energy for a small displacement dx of the interface MTM in the direction along the tube length. The energy balance equation then relates the entry radius of curvature r_{ow} given by Eq. (12) to the cross-sectional area exposed to change of fluid occupancy, A_{ow}, the bounding cross-sectional fluid-solid and fluid-fluid lengths, L_{sow} and L_{fow}, respectively, and the contact angle θ_{ow} indicated in Fig. 9. Because of symmetry of the regular star-shaped pore, we just consider one half of a corner of a pore.

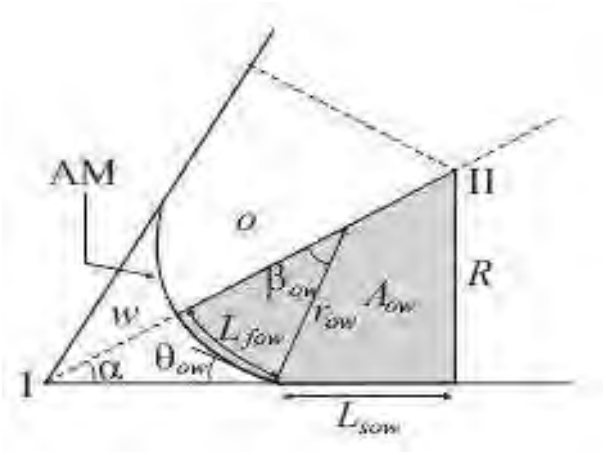

FIGURE 9. Corner of a tube showing parameters needed for calculating the capillary entry pressure, [4].

To displace the MTM a distance dx along the tube length, the virtual work required is given by

$$W_{ext} = P_{cow} A_{ow} dx. \tag{27}$$

The increase of surface free energy accompanying this displacement is given by

$$dF = \{(\sigma_{os} - \sigma_{ws}) L_{sow} + \sigma_{ow} L_{fow}\} dx \tag{28}$$

By using the energy balance equation given by $W_{ext} = dF$, we obtain

$$P_{cow} A_{ow} = \sigma_{ow} (L_{fow} + \cos\theta_{ow} L_{sow}), \tag{29}$$

where we have eliminated the fluid-solid interfacial tensions, σ_{os} and σ_{ws}, by using Eq. (1). Eq. (29) expresses the balance between the work done by the pressure difference on both phases and the energy difference associated with the creation and the removal of a portion of the area along the interfaces. By substituting Eq. (12) into Eq. (29) we obtain an expression for the radius of curvature r_{ow}, at which a displacement can take place, relating it to the geometry of the pore:

$$r_{ow} = \frac{A_{ow}}{L_{sow} \cos\theta_{ow} + L_{fow}}. \tag{30}$$

With the radius found from Eq. (30), for a given contact angle θ_{ow} and the corresponding capillary cross-sectional geometry, the capillary entry pressure can then be expressed in terms of the parameters involved and the interfacial tension by using the Young-Laplace equation again. To calculate the radius of curvature in Eq. (30) we need to study Fig. 9 to find expressions for the parameters involved.

The fluid-solid length, L_{sow}, is found by subtracting the distance of the pore wall still occupied by water from the total length d of the corner of the star-shaped pore given by (9).

This gives

$$L_{sow} = d - \frac{r_{ow}\sin\beta_{ow}}{\sin\alpha}, \tag{31}$$

where the angle β_{ow} is given by

$$\beta_{ow} = \frac{\pi}{2} - \alpha - \theta_{ow}. \tag{32}$$

The length of the arc of the fluid-fluid interface, L_{fow}, is

$$L_{fow} = r_{ow}\beta_{ow}. \tag{33}$$

The area occupied by oil, A_{ow}, is found by subtracting the area of the triangle with the two corners α and β_{ow} from the total area A of the half corner of the tube, given by (8), and then adding back the β-fraction of the circle with radius r_{ow}. In the calculation of the area of the triangle with the corners α and β_{ow} we have used the relation $\sin x\cos y+\cos x\sin y = \sin(x+y)$. The area occupied by oil is therefore

$$A_{ow} = A - \frac{r_{ow}^2\sin\beta_{ow}\sin(\alpha+\beta_{ow})}{2\sin\alpha} + \frac{r_{ow}^2\beta_{ow}}{2}. \tag{34}$$

Having defined the necessary parameters (31) - (34) for calculating r_{ow}, inserted into (30) it gives

$$r_{ow} = \frac{A - \frac{r_{ow}^2\sin\beta_{ow}\sin(\alpha+\beta_{ow})}{2\sin\alpha} + \frac{r_{ow}^2\beta_{ow}}{2}}{(d - \frac{r_{ow}\sin\beta_{ow}}{\sin\alpha})\cos\theta_{ow} + r_{ow}\beta_{ow}}, \tag{35}$$

From (35) we obtain the following second order polynomial to be solved for r_{ow}:

$$\Big(\frac{1}{2}\beta_{ow} - \frac{\sin\beta_{ow}\cos\theta_{ow}}{\sin\alpha} + \frac{\sin\beta_{ow}\sin(\alpha+\beta_{ow})}{2\sin\alpha}\Big)r_{ow}^2 + d\cos\theta_{ow}r_{ow} - A = 0,$$

or in a simpler form

$$\Big(\frac{1}{2}\beta_{ow} - \frac{1}{2}\frac{\sin\beta_{ow}\cos\theta_{ow}}{\sin\alpha}\Big)r_{ow}^2 + d\cos\theta_{ow}r_{ow} - A = 0, \tag{36}$$

since $\sin(\alpha+\beta_{ow}) = \cos(\theta_{ow})$. The solution for r_{ow} is given by

$$r_{ow} = \frac{-d\cos\theta_{ow} \pm \sqrt{(d\cos\theta_{ow})^2 - 4\Big(\frac{1}{2}\beta_{ow} - \frac{1}{2}\frac{\sin\beta_{ow}\cos\theta_{ow}}{\sin\alpha}\Big)(-A)}}{2(\frac{1}{2}\beta_{ow} - \frac{1}{2}\frac{\sin\beta_{ow}\cos\theta_{ow}}{\sin\alpha})},$$

or

$$r_{ow} = \frac{-d\cos\theta_{ow} \pm \sqrt{d^2\cos^2\theta_{ow} + 2A\Big(\beta_{ow} - \frac{\sin\beta_{ow}\cos\theta_{ow}}{\sin\alpha}\Big)}}{\beta_{ow} - \frac{\sin\beta_{ow}\cos\theta_{ow}}{\sin\alpha}}. \tag{37}$$

By using the relation $(a+b) = \frac{(a^2-b^2)}{(a-b)}$ with $a = -d\cos\theta_{ow}$ and $b = \sqrt{d^2\cos^2\theta_{ow} + 2A\Big(\beta_{ow} - \frac{\sin\beta_{ow}\cos\theta_{ow}}{\sin\alpha}\Big)}$, and choosing the physical relevant solution,

the radius r_{ow} of curvature is now given by

$$r_{ow} = \frac{2A}{d\cos\theta_{ow} + \sqrt{d^2\cos^2\theta_{ow} + 2A\Big(\beta_{ow} - \frac{\sin\beta_{ow}\cos\theta_{ow}}{\sin\alpha}\Big)}}, \tag{38}$$

or since $\sin\beta_{ow} = \cos(\alpha + \theta_{ow})$

$$r_{ow} = \frac{2A}{d\cos\theta_{ow} + \sqrt{d^2\cos^2\theta_{ow} - 2A\Big(\theta_{ow} - \frac{\pi}{2} + \alpha - \frac{1}{2}\sin 2\theta_{ow} + \frac{\cos^2\theta_{ow}}{\tan\alpha}\Big)}}, \tag{39}$$

where we have used the relations $\cos(x+y) = \cos x\cos y - \sin x\sin y$ and $\sin 2x = 2\sin x\cos x$.

Finally, by applying Young-Laplace equation (12) again, with r_{ow} from (39) and $\theta_{ow} = \theta_{pd}$, we obtain the following expression for the capillary entry pressure for primary drainage for a regular n-cornered star-shaped pore

$$Pc^{pd}_{\text{entry}} = \frac{\sigma_{ow}}{2A}\Big[d\cos\theta_{pd} + \sqrt{d^2\cos^2\theta_{pd} - 2A\Big(\theta_{pd} - \frac{\pi}{2} + \alpha - \frac{1}{2}\sin 2\theta_{pd} + \frac{\cos^2\theta_{pd}}{\tan\alpha}\Big)}\Big], \tag{40}$$

where A and d are given by (8) and (9) respectively. With $n = 3$ in (8) and (9), (40) applies for regular star-shaped pores with three-corners.

Case (2): In the case where $\theta_{ow} \geq \frac{\pi}{2} - \alpha$, the entire cross-section of a pore is filled with oil after invasion, and an AM is not formed. If $\theta_{ow} = \frac{\pi}{2} - \alpha$, the AM will touch the apex of the corner exactly. When there is no wetting fluid in the corners, the length of the fluid-solid interface L_{sow} equals the total length of the side d of the pore given by (9) that is

$$L_{sow} = d = \frac{R\sin\frac{\pi}{n}}{\sin\alpha}. \tag{41}$$

As no AM's forms, the length

$$L_{fow} = 0, \tag{42}$$

and the area occupied by oil equals the total area of the half corner given by (8), i.e.

$$A_{ow} = A = \frac{R^2}{2}\frac{\sin(\alpha + \frac{\pi}{n})\sin\frac{\pi}{n}}{\sin\alpha}. \tag{43}$$

By inserting (41) and (43) into the energy balance equation (29) the capillary pressure required for this event is given by

$$Pc_{ow} = \frac{\sigma_{ow}\cos\theta_{ow}d}{A}, \tag{44}$$

or with $n = 3$ for a three-cornered star shaped pore

$$Pc_{ow} = \frac{2\sigma_{ow}\cos\theta_{ow}}{R\sin(\alpha + \frac{\pi}{3})}. \tag{45}$$

Capillary entry pressures relevant for imbibition. We will now describe the procedure for determining the necessary capillary entry pressures relevant for the fluid displacements during imbibition indicated in Section 2.1, [2, 4], see Fig.3. If more than one displacement from configuration C is possible, the change of configuration connected with the highest capillary entry pressure is obtained.

In the following considerations, we use the notation shown in Fig. 10. The A_{ow} in (34) is here denoted by A_{ow1}, and represents the cross-sectional bulk area bounded by the only AM, now called AM1, in configurations B and C, and the outermost AM in configuration E. The contact angle θ_{ow} in (32) is here denoted by θ_1, and may be equal to θ_h given by (20) in configuration C and E, or θ_a in configuration B. The displacement from C to E results in the formation of an additional AM which will be denoted by AM2. The cross-sectional bulk areas bounded by AM1 and AM2, A_{ow1} and A_{ow2}, see Fig. 10, may now be expressed by

$$A_{ow1} = A - \frac{rb_1 \sin(\beta_1 + \alpha)}{2} + \frac{r^2\beta_1}{2}, \tag{46}$$

where

$$\beta_1 = \frac{\pi}{2} - \alpha - \theta_1, \tag{47}$$

and

$$A_{ow2} = A - \frac{rb_2 \sin(\beta_2 - \alpha)}{2} - \frac{r^2\beta_2}{2}, \tag{48}$$

where

$$\beta_2 = \frac{\pi}{2} + \alpha - \theta_2. \tag{49}$$

The cross-sectional oil-water and solid-fluid lengths shown in Fig. 10 are

$$L_{fi} = r\beta_i \quad \text{and} \quad L_{si} = d - b_i, \qquad i = 1, 2, \tag{50}$$

where

$$b_i = \frac{r \sin\beta_i}{\sin\alpha}, \qquad i = 1, 2. \tag{51}$$

Calculations of the capillary entry pressures for the fluid displacements during imbibition are done as follows:

$C \to B$. The displacement from C to B happens if the hinging contact angle given by (20) reaches θ_a before the capillary entry pressure for a displacement from C to D is reached. The AM's will move along the surface of altered wettability with the constant contact angle θ_a. The capillary pressure connected with this displacement is

$$Pc^{C\to B} = \frac{\cos(\theta_a + \alpha)}{\cos(\theta_{pd} + \alpha)} Pc^{max}. \tag{52}$$

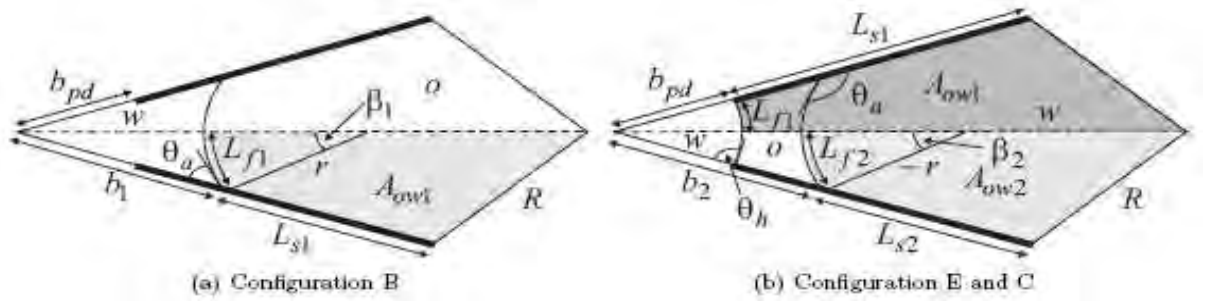

FIGURE 10. Illustration of the parameters used in describing the configurations B, C and E, [4].

$B \to D$**.** For a following change in configuration from B to D, the capillary entry pressure is given by

$$Pc_{\text{entry}}^{B\to D} = \frac{\sigma_{ow}}{2A}\Big[d\cos\theta_a + \sqrt{d^2\cos^2\theta_a - 2A\Big(\theta_a - \frac{\pi}{2} + \alpha - \frac{1}{2}\sin 2\theta_a + \frac{\cos^2\theta_a}{\tan\alpha}\Big)}\Big]. \tag{53}$$

This is found from solving the second order polynomial of r obtained from

$$r = \frac{A_{ow1}}{L_{s1}\cos\theta_a + L_{f1}}, \tag{54}$$

where $\theta_1 = \theta_a$. We note that this is the equivalent of solving (30), but with $\theta_{ow} = \theta_a$ in (30) and (32).

$C \to D$**.** For a displacement from C to D, we must solve Eq. (54) to find the entry radius of curvature, but in this case numerically because $\theta_1 \neq \theta_a$ in (47). Taking $r = R$ as the initial guess, β_1 is calculated from (51) with $b_1 = b_{pd}$. The next step is to calculate the quantities of Eq. (54) from (46) and (50), and thus by (54) a new estimate of r is obtained. By iteratively repeating the indicated procedure, the entry pressure is at last given by

$$Pc_{\text{entry}}^{C\to D} = \frac{\sigma_{ow}}{r}. \tag{55}$$

$C \to E$**.** For a displacement from C to E, r is given by

$$r = \frac{A_{ow2}}{L_{s2}\cos\theta_a - L_{f2}}. \tag{56}$$

By using (48) – (51), this yields a second order polynomial that has to be solved for r. The capillary entry pressure corresponding to the physically correct root is given by

$$Pc_{\text{entry}}^{C\to E} = \frac{\sigma_{ow}}{2A}\Big[d\cos\theta_a - \sqrt{d^2\cos^2\theta_a + 2A\Big(\theta_a - \frac{\pi}{2} - \alpha - \frac{1}{2}\sin 2\theta_a - \frac{\cos^2\theta_a}{\tan\alpha}\Big)}\Big]. \tag{57}$$

$E \rightarrow D$**.** For a following change of configuration from E to D, the relevant expression for r is

$$r = \frac{A_{ow1} - A_{ow2}}{(L_{s1} - L_{s2})\cos\theta_a + L_{f1} + L_{f2}}. \tag{58}$$

With $b_1 = b_{pd}$ and $\theta_2 = \theta_a$, and using (46) – (51), we arrive at

$$\pi - \theta_a - \theta_1 + \cos\theta_a \frac{\cos(\theta_a - \alpha)}{\sin\alpha} + (\cos\theta_1 - 2\cos\theta_a)\frac{\cos(\theta_1 + \alpha)}{\sin\alpha} = 0. \tag{59}$$

Solving Eq. (59) numerically for θ_1 taking $\theta_1 = \theta_a$ as the initial value, we finally use the converged value of θ_1 together with (47), (51) and (12) to calculate the capillary entry pressure $Pc_{\text{entry}}^{E\rightarrow D}$.

3. A capillary pressure correlation for mixed oil-water wet conditions

The former correlation. Skjaeveland et al. [11] have published a general capillary pressure correlation for mixed-wet reservoir rock. The suggested expression correlates the capillary pressure with the water saturation and covers primary drainage, imbibition, secondary drainage and hysteresis scanning loops.

The correlation is the sum of two terms

$$P_c = \frac{c_w}{\left[\frac{S_w - S_{wr}}{1 - S_{wr}}\right]^{a_w}} + \frac{c_o}{\left[\frac{S_o - S_{or}}{1 - S_{or}}\right]^{a_o}}, \tag{60}$$

which correspond to a water-wet branch and an oil-wet branch, respectively. The a_w, a_o and c_w are positive constants and c_o is a negative constant. There is one set of constants for imbibition and one set for drainage. S_{wr} denotes the residual water saturation and S_{or} the residual oil saturation. The graph of Eq. (60), both for imbibition and drainage, thus consists of a positive water branch with an asymptote at $S_w = S_{wr}$ and a negative oil branch with an asymptote at $S_w = S_{or}$, see Fig. 11 taken from [11]. For primary drainage of a completely water-wet reservoir (i.e. the process of reducing the water saturation from $S_w = 1$) the capillary pressure is expressed by the first term of Eq. (60).

The figure shows the primary drainage curve, denoted as (a), obtained by starting at $S_w = 1$ where $c_o = 0$ and c_w equals to the entry pressure. For primary imbibition of a completely oil-wet rock (i.e. the process of reducing the oil saturation from $S_o = 1$), the capillary pressure is expressed by the second term. The primary imbibition curve (d) is thus modeled with $c_w = 0$, and c_o is now equal to the entry pressure of water into a 100% oil saturated core. For the intermediate cases, the capillary pressure is the sum of the two terms. The figure also shows the bounding (secondary) imbibition (b) and secondary drainage curves (c) forming the largest possible hysteresis loop.

The modified correlation. Now, the authors of [11] have extended the correlation to model fluid flow processes where the wettability may change with time. The suggested correlation given in [12] takes the following form:

$$Pc(S_w, \theta) = \frac{c_w \cos(\theta/2)}{\left[\frac{S_w - S_{wr}}{1 - S_{wr}}\right]^{a_w}} + \frac{c_o \cos((\pi + \theta)/2)}{\left[\frac{S_o - S_{or}}{1 - S_{or}}\right]^{a_o}}. \tag{61}$$

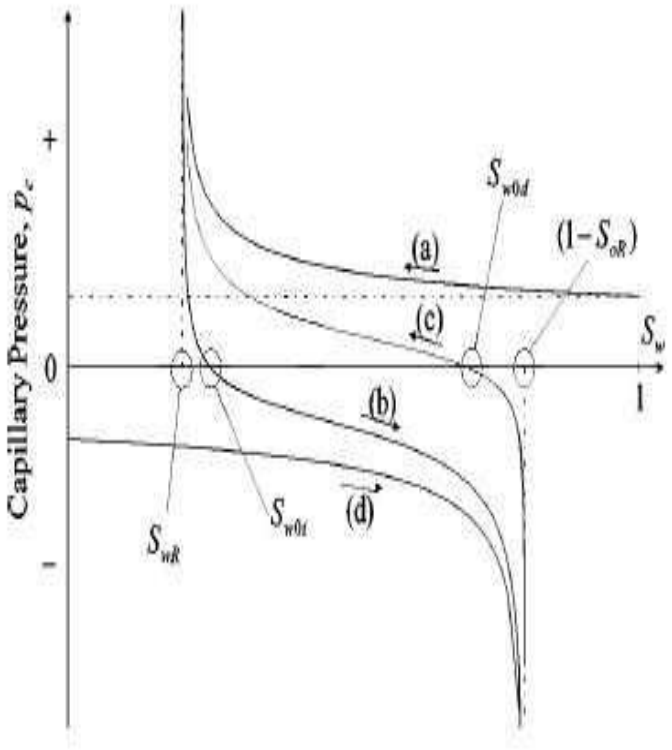

FIGURE 11. The capillary pressure Pc, given by Eq. (60), as a function of the wetting phase saturation, S_w, for: (a) primary drainage; (b) (secondary) imbibition; (c) secondary drainage and (d) primary imbibition.

In particular, the new parameter $\theta \in [0, \pi]$ is an *averaged* contact angle expressing the wettability of the porous media in question. The parameters c_w, a_w, c_o and a_o are now positive constants. This expression also consists of a water-wet branch and an oil-wet branch. Transition between water-wet and oil-wet conditions is obtained by varying the contact angle θ. In general, the residual saturations S_{wr} and S_{or} depend on θ. For the cases where changes of interfacial tension plays an important role, the formulas for capillary pressure are modified by multiplying the numerators in Eq. (61) by the interfacial tension σ [12].

Fig. 12 shows four sets of curves of $Pc(S_w, \theta)$ generated from the suggested correlation (61) for different choices of the unknown parameters c_w, c_o, a_w and a_o. An individual curve in each of the three examples corresponds to a contact angle θ in the range $[40°, 180°]$ which is the interval we have chosen for θ_a in the pore model. The residual saturations S_{wr} and S_{or} have been set to 0.01.

If we compare the left and right plots of Fig. 12 it is clear that the size of the parameters a_w and a_o influence the behavior of the curves near the end points $S_w = 0, 1$. Comparing

the top and bottom plots it is clear that the values of c_w and c_o determine the spreading of the curves for different contact angles.

4. Validation of the correlation by using the pore scale model

The purpose of this section is to discuss how the correlation (61) possibly can be evaluated by making use of the pore scale model described in Section 2. In other words, we want to employ the pore scale model as a tool for visualizing the pore structure of a porous media that can be represented well by the capillary pressure correlation given by Eq. (61). In the following we focus exclusively on the imbibition process. As a first approach the following simplifying assumptions are made:

- We consider the case $S_{wr} = S_{or} = 0.01$. This correspond to the values obtained at the end of primary drainage in the pore model. Generally, the residual saturations are positive and depend on both averaged contact angle θ and interfacial tension;

- c_w and c_o are assumed to be constants. In a more general setting dependence on interfacial tension could be included.

Since a specific wetting state is represented by a distribution $\theta_a(R)$ of advancing contact angles in the pore scale model, whereas the same wetting state is represented by an averaged contact angle θ in the correlation (61), it is crucial to define a precise rule that relates $\theta_a(R)$ and θ. One way to express this is to define a family of $\theta_a(R)$, one for each $\theta \in [\theta_{min}, \theta_{max}]$. This gives rise to a two-variable function $\theta_a(R, \theta)$. Consistent with Eq. (21), we have

$$\theta_a(R, \theta) \overset{\text{Pore model}}{\longrightarrow} Pc^{Pore}(S_w, \theta). \tag{62}$$

An important task is to describe the function $\theta_a(R, \theta)$. In the remaining part of this section we consider two different choices of $\theta_a(R, \theta)$. Firstly, we use a straightforward relation between θ_a and θ where θ_a is directly associated with θ. No specific information from the pore model is taken into account in this relation (e.g. no detailed information at the pore level is accounted for). Secondly, we define $\theta_a(R, \theta)$ such that the distribution $\theta_a(R, \theta)$ and the corresponding θ satisfies a Cassie's law type of relation. Consequently, we use a relation where information about the area of the pores with altered wettability is considered.

For a given choice of $\theta_a(R, \theta)$ we compare the produced corresponding capillary pressure function $Pc^{Pore}(S_w, \theta)$ with the correlation $Pc^{Corr}(S_w, \theta)$ given by (61). In particular, we use an optimization algorithm to find the unknown parameters c_w, a_w, c_o and a_o that minimize the difference between $Pc^{Pore}(S_w, \theta)$ and $Pc^{Corr}(S_w, \theta)$. Through this procedure we seek to identify a pore scale description whose capillary pressure function Pc^{Pore} gives a good match with the correlation Pc^{Corr}.

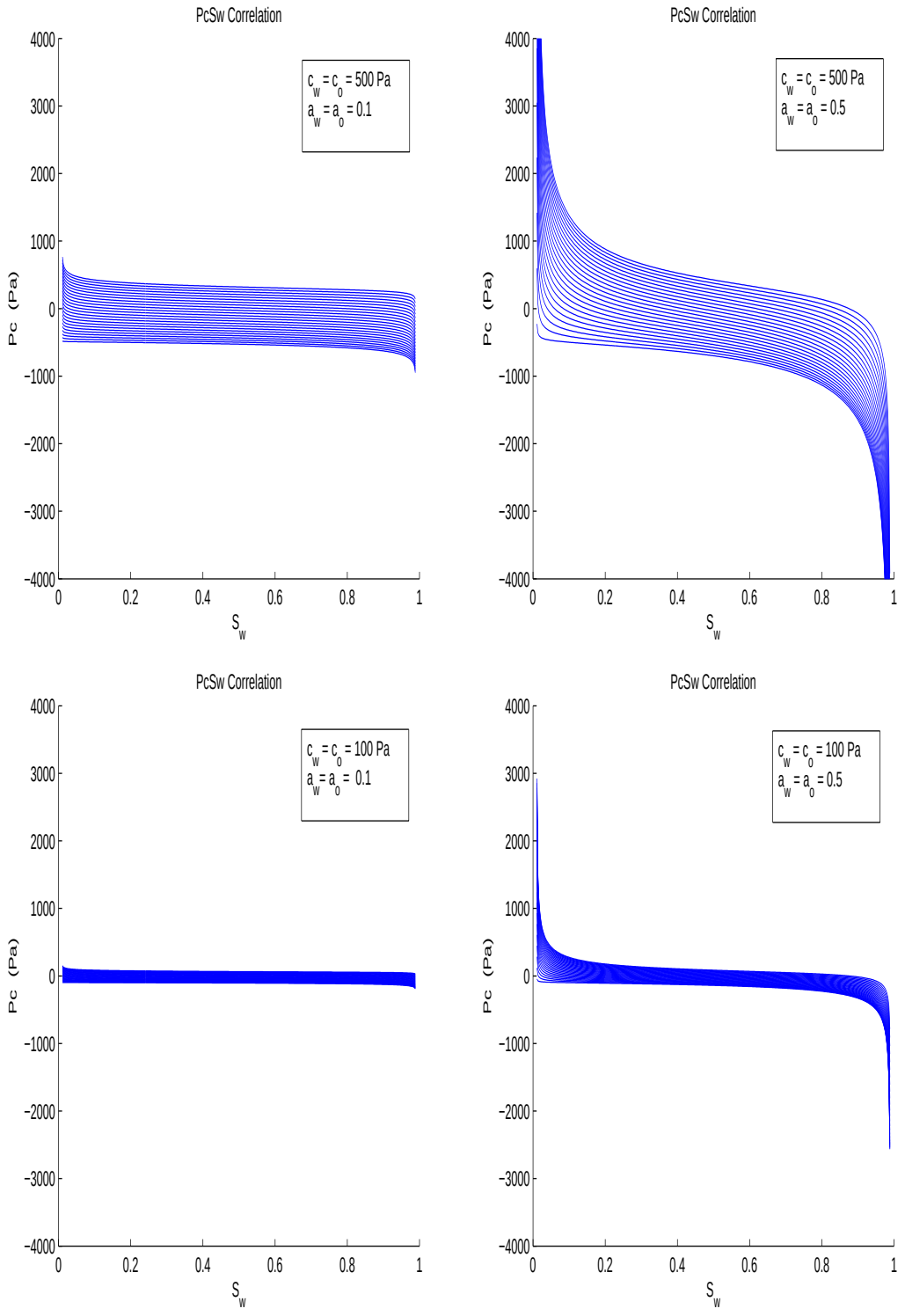

FIGURE 12. $Pc(S_w)$ generated by the correlation for different $\theta \in [40°, 180°]$ and with different values of the parameters c_w, c_o, a_w and a_o..

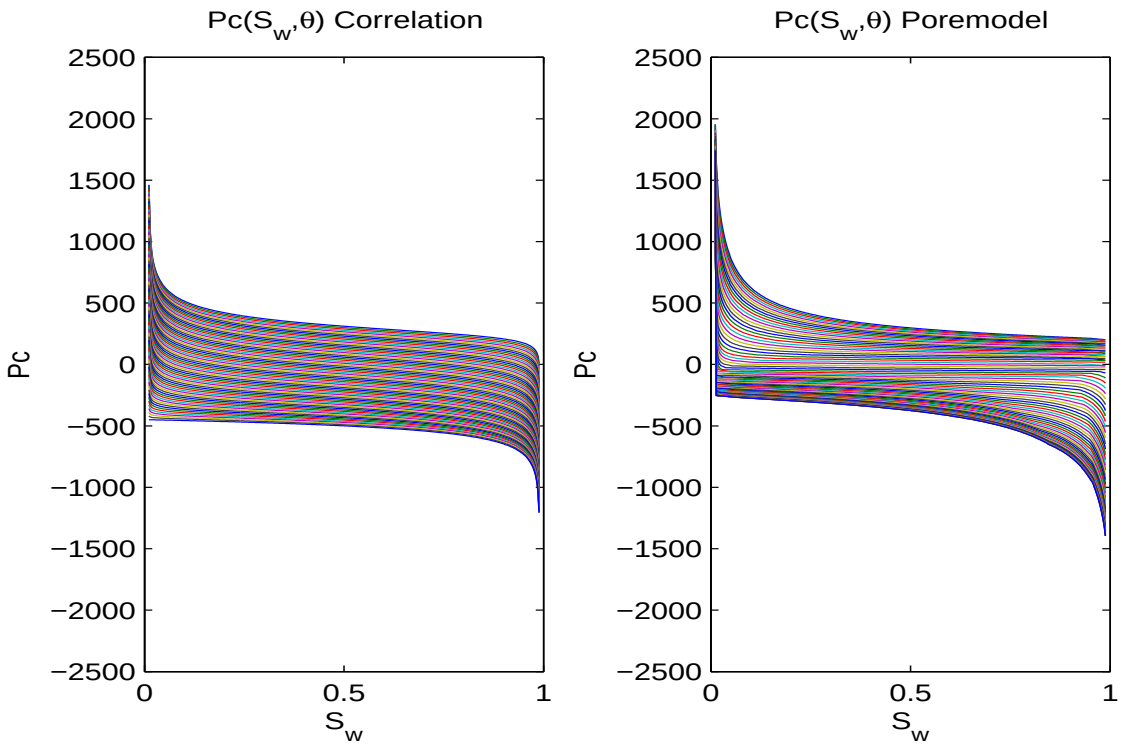

FIGURE 13. **Example 1a): Left:** $Pc^{\mathrm{Corr}}(S_w)$ generated from the correlation (61) with the estimated parameters given by (68). **Right:** $Pc^{\mathrm{Pore}}(S_w)$ generated from the pore model by using $\theta_a(R,\theta)$ given by (63). In both cases Pc is plotted for the different $\theta \in [\theta_{\min}, \theta_{\max}]$.

4.1. **Case I: A simple expression for relating the averaged contact angle θ to a corresponding wetting state $\theta_a(R,\theta)$ in the pore model.** As described in section 2.1, the wetting state in the pore model during imbibition is described by the assigned distribution of different local contact angles θ_a to the different tubes, in proportion to their size.

We will now consider the special case where the averaged contact angle θ, representing the wetting state in the porous media, is related to the pore distribution $\theta_a(R,\theta)$ by the simple linear relation

$$\theta_a(R,\theta) = \theta, \qquad (R,\theta) \in [R_{\min}, R_{\max}] \times [\theta_{\min}, \theta_{\max}]. \tag{63}$$

In other words, the pore contact angles $\theta_a(R)$ are the same for all different pores, and coincide with the averaged contact angle θ. Having defined this relation between $\theta_a(R,\theta)$ and θ, we are now in the position where we can compare $Pc^{\mathrm{Pore}}(S_w,\theta)$, generated by the pore model, with $Pc^{\mathrm{Corr}}(S_w,\theta)$ generated by the correlation (61). In particular, we want to explore to what extent Pc^{Corr} can be used to represent Pc^{Pore}. That is, to find good

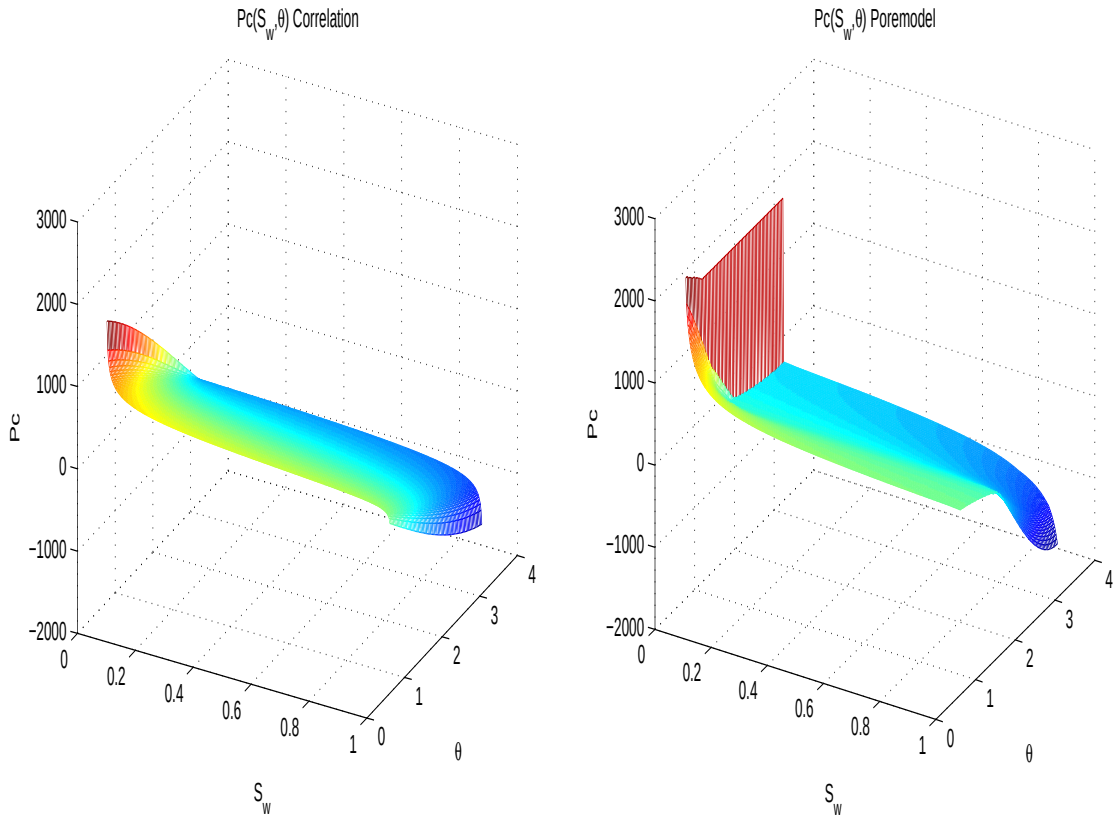

FIGURE 14. **Example 1a**: **Left:** $Pc^{\text{Corr}}(S_w, \theta)$ generated from the correlation (61) with the estimated parameters given by (68). **Right:** $Pc^{\text{Pore}}(S_w, \theta)$ generated from the pore model by using $\theta_a(R, \theta)$ given by (63).

choices of the parameters c_w, a_w, c_o and a_o in (61) such that the difference between the two curves is minimized.

To estimate the four parameters in the correlation, c_w, a_w, c_o and a_o, we have used the MATLAB function *lsqcurvefit* from the 'Optimization Toolbox'. This function solves nonlinear curve-fitting (data-fitting) problems in the least-squares sense. That is, given input data xdata and ydata, and the observed output zdata, we can find coefficients (parameters) k that "best fit" the equation

$$\min_{k\in K} \Big\| F(k, \text{xdata}, \text{ydata}) - \text{zdata} \Big\|_2^2 := \min_{k\in K} \int_{x_{min}}^{x_{max}} \int_{y_{min}}^{y_{max}} \Big(F(k, \text{xdata}, \text{ydata}) - \text{zdata} \Big)^2 dydx. \tag{64}$$

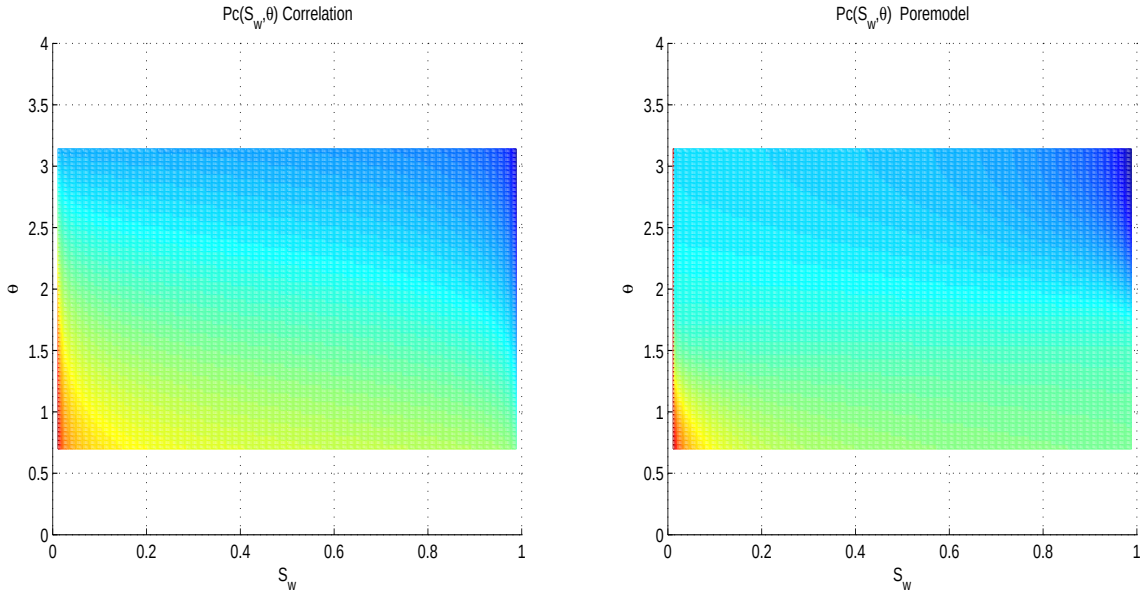

FIGURE 15. **Example 1a)**: The curves shown in Fig. 14 seen from above.

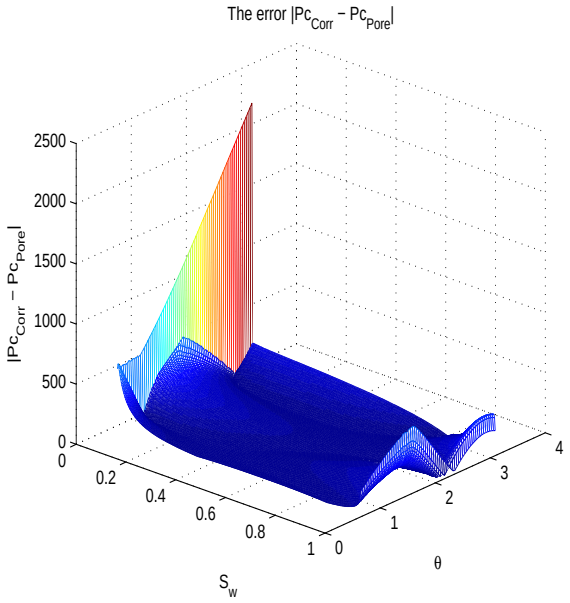

FIGURE 16. **Example 1a):** The error $E = |Pc^{\mathrm{Corr}}(S_w, \theta) - Pc^{\mathrm{Pore}}(S_w, \theta)|$ for the curves in Fig. 14.

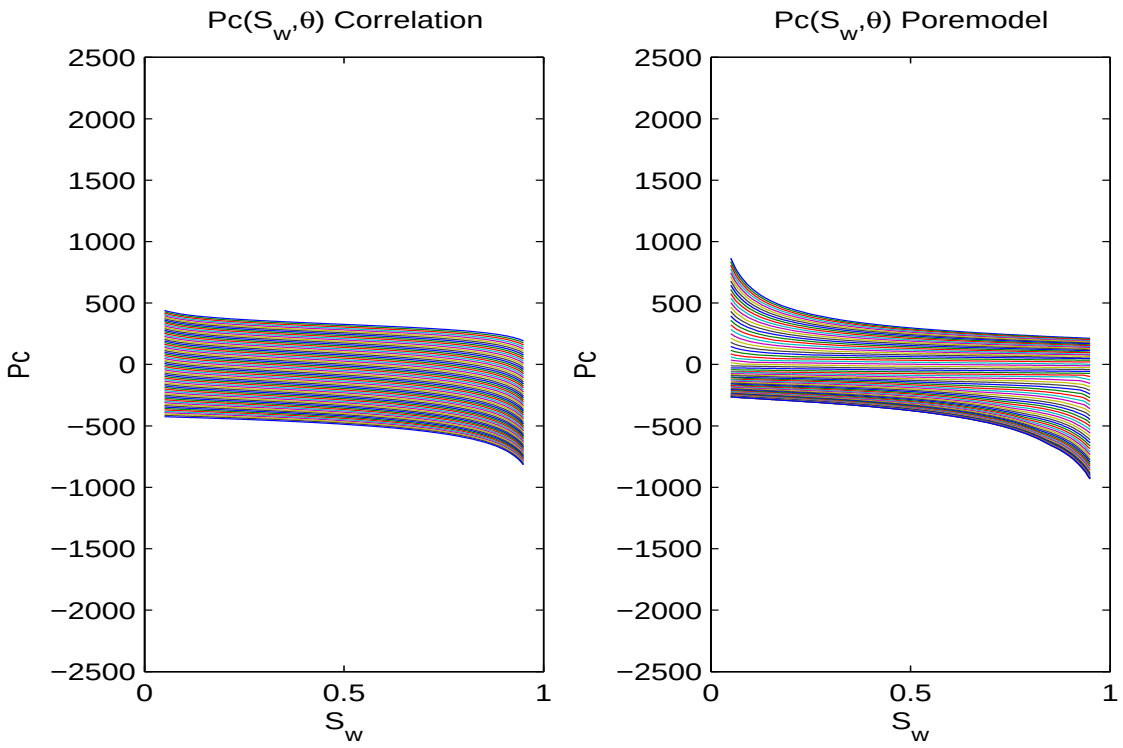

FIGURE 17. **Example 1b)**: Plots of the same curves as in Fig. 13 with a reduced saturation interval.

Here K represents the parameter space, that is, the region in which the parameter vector can lie. The xdata and ydata are matrices or vectors, and $F(x, \text{xdata}, \text{ydata})$ is a matrix-valued function. The F function in our case is of course the correlation $Pc^{\text{Corr}}(S_w, \theta)$ given in Eq. (61). The saturation interval amounts to the xdata, and is divided in the following way

$$\{S_{w,i}\}_{i=1}^{m} \text{ where } S_{w,1} = S_{w,\min}, \quad S_{w,i} = S_{w,\min} + (i-1)\triangle S_w, \qquad i = 2, ..., m \\ \text{and } S_{w,m} = S_{w,\max}. \tag{65}$$

The different θ values amount to the ydata and have the uniform distribution:

$$\{\theta_j\}_{j=1}^{M} \text{ where } \theta_1 = \theta_{a,\min}, \quad \theta_j = \theta_{a,\min} + (j-1)\triangle\theta, \qquad j = 2, ..., M-1 \\ \text{and } \theta_M = \theta_{a,\max}, \tag{66}$$

where $\triangle\theta_a = (\theta_{a_{max}} - \theta_{a_{min}})/(M-1)$. For every pair of $(\theta_j, S_{w,i})$ we have calculated the corresponding value of Pc from the pore model by means of an interpolation routine. These Pc-values now amount to the observed output zdata in Eq. (64). The least squares problem in our case is therefore

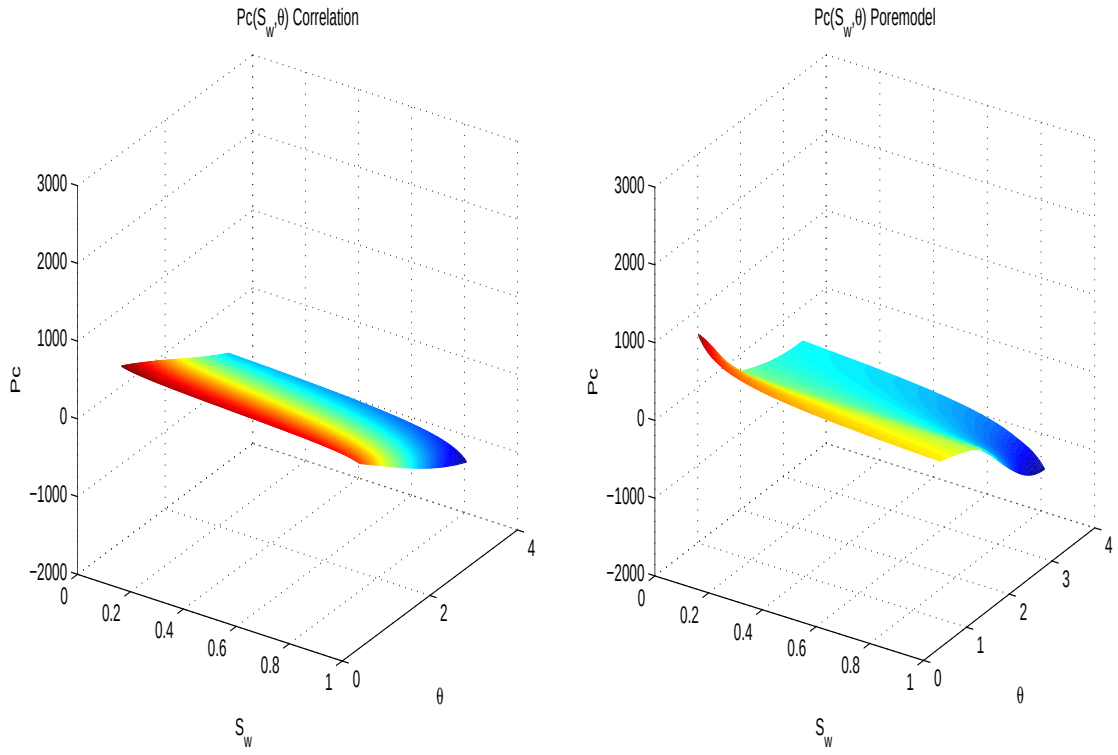

FIGURE 18. **Example 1b)**: Plots of the same curves as in Fig. 14 with a reduced saturation interval.

$$\min_{k\in K}\left\|F(k,S_w,\theta)-Pc^{\text{Pore}}\right\|_2^2 \tag{67}$$
$$=\min_{k\in K}\int_0^1\int_{\theta_{a,\min}}^{\theta_{a,\max}}\left(Pc^{\text{Corr}}(S_w,\theta;c_w,a_w,c_o,a_o)-Pc^{\text{Pore}}(S_w,\theta)\right)^2 d\theta dS,$$

where $k=[c_w\ a_w\ c_o\ a_o]$.

We have used the algorithm [k,resnorm] = lsqcurvefit(fun,k0,xdata,ydata,zdata) which returns the value of the squared 2-norm of the residual at k.

In Example 1a) and 1b) below, the curve-fitting is done in three steps. First, only the first term of the correlation in Eq. (61) is fitted for small S_w to estimate c_w and a_w. Next, the second term of the correlation is fitted for small S_o to estimate c_o and a_o. Then, all the four parameters are optimized simultaneously for both terms of Eq. (61) for the entire saturation range. This gives a better match with the pore model for this case. For Example 2a) and 2b) in section 4.3, the curve-fitting shows little or no difference when we do the curve-fitting in steps compared to doing it in one step only.

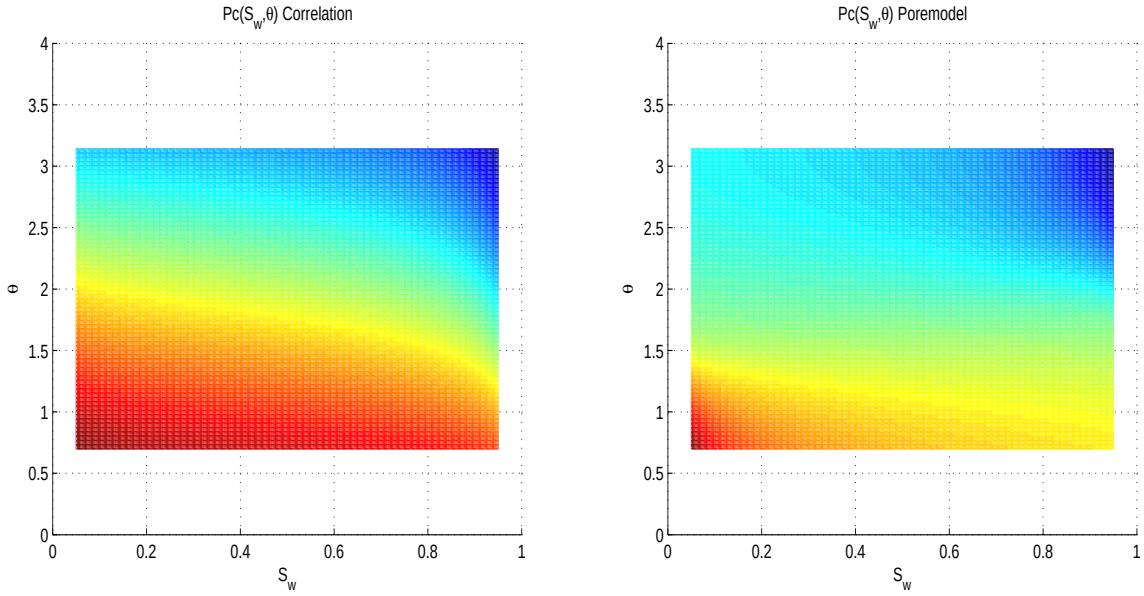

FIGURE 19. **Example 1b)**: The curves shown in Fig. 18 seen from above.

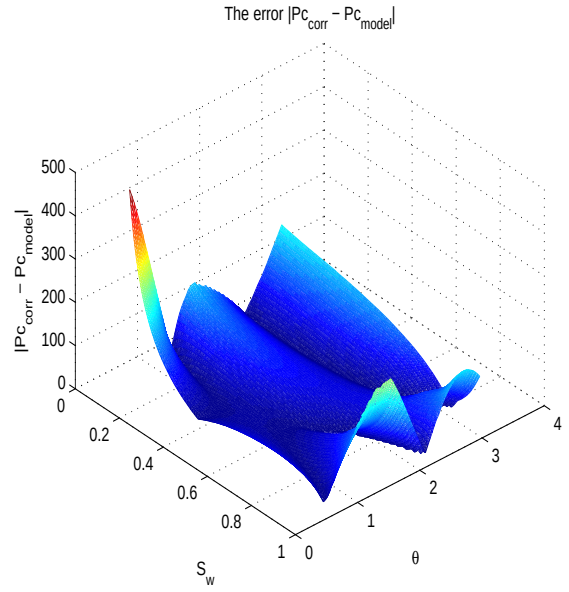

FIGURE 20. **Example 1b):** The error $E = |Pc^{\mathrm{Corr}}(S_w, \theta) - Pc^{\mathrm{Pore}}(S_w, \theta)|$ for the curves in Fig. 18.

4.2. **Assessment of the correlation for Case I.**

Example 1a). The saturation interval is defined from $S_{w,\min} = 0.011$ to $S_{w,\max} = 1-0.011$, where $\triangle S_w = 0.0025$ and $m = 393$. The contact angles are uniformly distributed with $\theta_{a,\min} = 40°$, $\theta_{a,\max} = 180°$, $\triangle\theta = 2°$ and $M = 71$.

The estimated parameters are as follows:

$$c_w = 447Pa, \qquad a_w = 0.20, \qquad c_o = 449Pa \qquad \text{and} \qquad a_o = 0.15. \tag{68}$$

A plot of Pc as a function of S_w for $\theta \in [\theta_{\min}, \theta_{\max}]$ generated by the correlation with the estimated parameters (68) is shown to the left in Fig. 13. To the right is shown a plot of the corresponding curves generated by the pore model based on $\theta_a(R, \theta)$ given by (63). 3D plots of the $Pc^{\text{Corr}}(S_w, \theta)$ and $Pc^{\text{Pore}}(S_w, \theta)$ curves are shown in Fig. 14. The 3D curves seen from above and a plot of the error $E = |Pc^{\text{Corr}}(S_w, \theta) - Pc^{\text{Pore}}(S_w, \theta)|$ are shown in Fig. 15 and Fig. 16 respectively.

Observations: In view of Fig. 13–16 we may remark:

- Fig.13 and 14 illustrate that the correlation does not capture so well the large and small Pc-values at the endpoints.
- Fig.13 also shows that for the highest values of θ, the curves generated by the correlation does not fit so well with the corresponding curves generated by the pore model.
- The error is relatively large for high values of θ together with small water saturations, see Fig.16.

Example 1b). To check how the correlation matches in a smaller saturation interval (i.e. we want to avoid the strong impact for small and large saturations), we reduce the interval by starting at $S_{w,\min} = 0.05$ and going to $S_{w,\max} = 1 - 0.05$. We then get the following estimated parameters:

$$c_w = 500Pa, \qquad a_w = 0.07, \qquad c_o = 421Pa \qquad \text{and} \qquad a_o = 0.21. \tag{69}$$

Fig. 17 shows the $Pc(S_w)$ curves (where Pc is plotted as a function of S_w for $\theta \in [\theta_{\min}, \theta_{\max}]$) generated by the correlation with the estimated parameters (69) to the left, and by the pore model to the right. 3D plots of the $Pc^{\text{Corr}}(S_w, \theta)$ and $Pc^{\text{Pore}}(S_w, \theta)$ curves are shown in Fig. 18. In Fig. 19 the 3D plots are seen from above and he error $E = |Pc^{\text{Corr}}(S_w, \theta) - Pc^{\text{Pore}}(S_w, \theta)|$ is illustrated in Fig. 20.

Observations: In view of Fig. 17–20 we remark:

- The estimated parameters have changed as follows: c_w is higher while a_w and c_o are smaller. a_o is unchanged.
- The correlation still doesn't bring forth the large and small Pc-values at the endpoints.
- We also here observe a relatively poor fit for the curves generated by the correlation for the highest values of θ.

- In contrast to the situation in Ex.1a) the error is now larger for the small values of θ combined with the lowest water saturations. The maximum error has been reduced from the order of 10^3 to the order of 10^2.

4.3. **Case II: An averaged contact angle motivated by Cassie's law.**

Cassie's law for modeling the contact angle on chemically heterogeneous surfaces. As mentioned is Section 1.1, Eq. (1), the oil-water contact angle on an ideal surface is expressed by Young's relation which is reproduced here as:

$$\cos\theta_{lg} = \frac{\sigma_{sg} - \sigma_{sl}}{\sigma_{lg}}. \tag{70}$$

This relation was developed for the case of an ideal solid surface, which is smooth and chemically homogeneous. In reality, of course, the solid surfaces in porous media are typically both heterogeneous and rough to some extent. To allow for non-ideal surfaces, the averaged effective contact angle applied in the correlation presented in Eq. (61) has to take the different conditions into account. In the following we will study the effect of heterogeneity of the solid surface on the averaged contact angle. That is, all other conditions that would influence the averaged contact angle (i.e. the roughness of the surface etc.) are neglected. On a chemically heterogeneous solid surface, the surface tensions vary from one local area to the other. Accordingly, the Young's contact angle has a different, local value at each area. In general, the surface can be characterized by a properly averaged apparent contact angle.

The most stable apparent contact angle on a heterogeneous surface θ is given by the well known Cassie's law [9] which was published in 1948. This equation suggests a way of modeling the contact angle of a macroscopic droplet on a heterogeneous surface with two different chemistries.

Cassie has shown that by averaging the surface energy, the contact angle of a heterogenous surface, which consists of two types of surfaces each characterized by its own contact angle ϕ_1 with areal fraction f_1 and ϕ_2 with areal fraction f_2, respectively, $(f_1 + f_2 = 1)$, is given by

$$\cos\theta_C = f_1\cos\phi_1 + f_2\cos\phi_2, \tag{71}$$

where θ_C denotes the contact angle calculated by Cassie's law. This equation can be generalized such that the cosine of the Cassie contact angle is the weighted average of the cosines of all the Young contact angles that characterizes the surface. That is, the apparent angle (which is restricted to the interval $([\phi_1, \phi_2])$) is given by an average involving the angles characteristic of each constituent, but the average is applied to the cosines of these angles. The weighted averaging is done according to the area fraction of each chemistry. For a chemically heterogeneous surface, the extended averaged Cassie's contact angle is then given by

$$\cos\theta_C = \sum_i f_i\cos\theta_i, \tag{72}$$

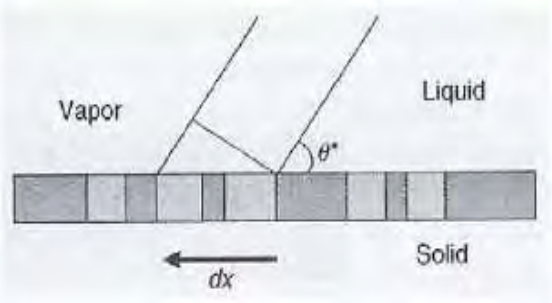

FIGURE 21. Edge of a drop placed on a chemically composite surface. We consider a small displacement dx (to the left) of the line of contact [5].

where θ_i is the angle taken on a simple planar surface component or chemical species i, f_i the fraction of area of the surface made up of i. Cassie equation is an approximation that becomes better when the drop size becomes larger with respect to the scale of chemical heterogeneity.

Cassie's law is obtained by considering the energy variation associated with a small displacement dx of a drop placed on a chemically composite surface, see Fig. 21 taken from [5]. We assume that the individual areas of the different types of surfaces are very small compared to the size of the drop. If we let θ^* denote the apparent contact angle, the energy variation combined with the displacement dx is

$$dE = f_1(\sigma_{sl} - \sigma_{sg})_1 \, dx + f_2(\sigma_{sl} - \sigma_{sg})_2 \, dx + \sigma_{lg} \, dx \, \cos\theta^*, \tag{73}$$

where the indices 1 and 2 refer to one or the other species swept during the displacement - species 1 with a probability f_1, and species 2 with a probability f_2.

The minimum of the energy E, i.e. $dE = 0$, together with the following form of Young's relation $\sigma_{sl} - \sigma_{sg} = -\sigma_{lg}\cos\theta_{lg}$ applied to each solid, now gives

$$\sigma_{lg} \, dx \, \cos\theta^* = f_1(-\sigma_{lg}\cos\theta_{lg})_1 dx + f_2(-\sigma_{lg}\cos\theta_{lg})_2 dx. \tag{74}$$

Since the interfacial tension σ_{lg} is constant, we arrive at

$$\cos\theta^* = f_1\cos\theta_{lg_1} + f_2\cos\theta_{lg_2} \tag{75}$$

which is Cassie's law, i.e $\theta^* = \theta_C$. Since the Eqs. (71) and (72) are derived from the thermodynamic definition of contact angle, the Cassie's angle θ_C, is therefore not an *observable* apparent contact angle but a *conceptual* effective contact angle. This means that Cassie's law cannot be applied to calculate the apparent contact angle but is instead a definition of the effective contact angle. In other words, the contact angle θ_C calculated from Cassie's law cannot be used to interpret the observed real contact angle on a heterogeneous surface. The Cassie's contact angle can only be compared to the ensemble average of the cosines of many contact angles at different positions on a heterogeneous surface.

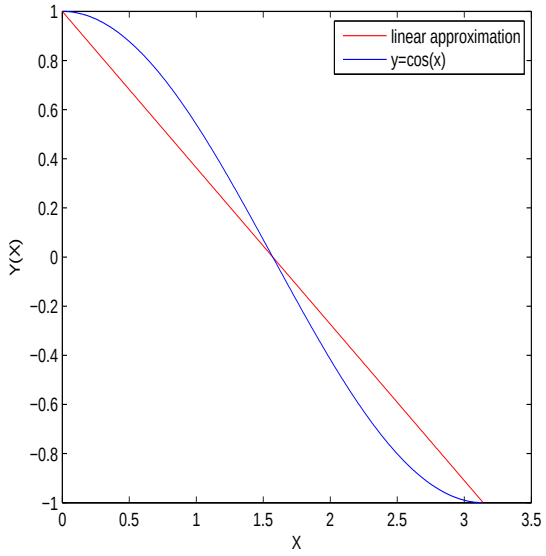

FIGURE 22. Linear approximation for $\cos(x)$.

Cassie's contact angle applied in combination with the correlation. In the following we want to investigate the use of Cassies contact angle in the correlation. More precisely, the purpose is to apply this contact angle as the effective contact angle θ expressing the wettability of the porous media. That is, we must define $\theta_a(R, \theta_C)$ such that for $\theta_C^* \in [\theta_{min}, \theta_{max}]$, θ_C^* and $\theta_a(R, \theta_C^*)$ obey Cassie's law.

In a discrete description where we have $\{R_i\}_{i=1}^N$ and $\{\theta_{C,j}\}_{j=1}^M$, this means that the following relation should hold:

$$\cos\theta_{C,j} = \sum_{i=1}^{N} f_i \cos\theta_a(R_i, \theta_{C,j}), \qquad j = 1, \ldots, M. \tag{76}$$

The other parameters f_i will be explained below. In addition, it is also instructive to consider a simplified form of Cassie's law where we leave out the cosine of the contact angles. This is motivated by the approximation

$$\cos(x) \approx -\frac{2}{\pi}x + 1, \qquad x \in [0, \pi]. \tag{77}$$

See Fig. 22 for an illustration. Inserting this approximation for $\cos\theta$ into Cassie's law gives

$$\begin{aligned}
(-\frac{2}{\pi}\theta+1) &= \sum_{i=1}^{N} f_i(-\frac{2}{\pi}\theta_a(R_i,\theta)+1) \\
-\frac{2}{\pi}\theta+1 &= \sum_{i=1}^{N} f_i(-\frac{2}{\pi}\theta_a(R_i,\theta)) + \sum_{i=1}^{N} f_i \\
-\frac{2}{\pi}\theta+1 &= -\frac{2}{\pi}\sum_{i=1}^{N} f_i\theta_a(R_i,\theta)+1 \\
\theta &= \sum_{i=1}^{N} f_i\theta_a(R_i,\theta),
\end{aligned} \tag{78}$$

since by definition $\sum_{i=1}^{N} f_i = 1$. That is, the relation in Eq. (78) suggests that the apparent contact angle θ is the weighted average of all the local contact angles $\theta_a(R_i,\theta)$ that characterize the heterogeneous surface. With this we mean that the relation between $\theta_a(R,\theta)$ and θ satisfies

$$\theta_{AC,j} = \sum_{i=1}^{N} f_i\theta_a(R_i,\theta_{AC,j}), \qquad j=1,\ldots,M. \tag{79}$$

Here θ_{AC} represents the averaged contact angle found by what we will call the *approximated Cassie's law* (79).

The following assumptions are made regarding the use of (76) and (79):

(i) The heterogeneous surface in question is associated with the bundle of tubes in the pore model representing the porous media. Each tube is regarded as a chemically different type of surface, and the effective contact angle we are searching is therefore an area average over the local contact angles of all the pores in the model.

(ii) The contributing area f_i for a single tube is the part of the pore walls with altered wettability at the end of primary drainage. In particular, we assume that the f_i's are constant for all wetting states, i.e. they are not affected by changes in the wetting state represented by θ_a.

The area f_i in question for a tube amounts to the area marked with bold lines in Fig. 4. We will still consider just one half of a corner of the regular star-shaped pores in the model, and the length of the pore walls of interest will be denoted by L_p. This length can be found by the length of the apex d of a corner in a pore from Eq. (9) and the water-wet distance b_{pd} in the corner of a tube defined in Eq. (18). L_p for a pore is then given by

$$L_p = d - b_{pd} = \frac{R\sin\frac{\pi}{n}}{\sin\alpha} - \frac{\sigma_{ow}\cos(\theta_{pd}+\alpha)}{Pc^{\max}\sin\alpha}. \tag{80}$$

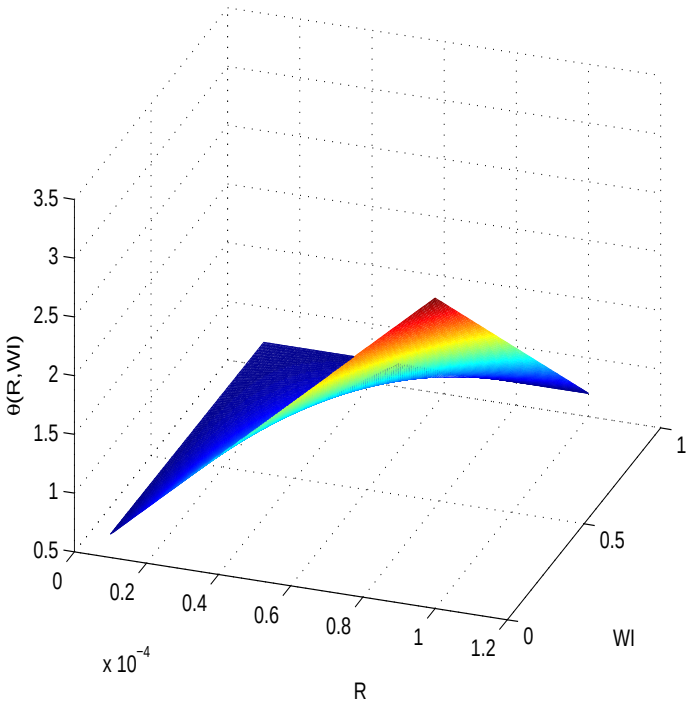

FIGURE 23. $\widetilde{\theta}_a(R, WI)$

For k tubes, the Cassie relation is therefore

$$\cos\theta_C = \frac{\sum_{i=1}^{k}(L_{p_i}\ \cos\theta_{a,i})}{L}, \tag{81}$$

where L is the total area of the surfaces L_p, i.e. $\frac{\sum_{i=1}^{k} L_{p_i}}{L} = 1$. Small tubes that have not yet been invaded by oil, are still strongly water-wet with no area with altered wettability and will therefore not contribute to the averaged contact angle in question. The equivalent of Eq. (81) for the simplified example is

$$\theta_{AC} = \frac{\sum_{i=1}^{k}(L_{p_i}\ \theta_{a,i})}{L}. \tag{82}$$

Construction of $\theta_a(R, \theta)$. What remains is to describe how to define the distribution $\theta_a(R, \theta)$ such that Cassie's law is taken into account in the following sense:

$$\cos(\theta_{C,j}) = \sum_{i=1}^{N} f_i \cos\theta_a(R_i, \theta_{C,j}), \tag{83}$$

for $j = 1, \ldots M$. We propose the following stepwise procedure.

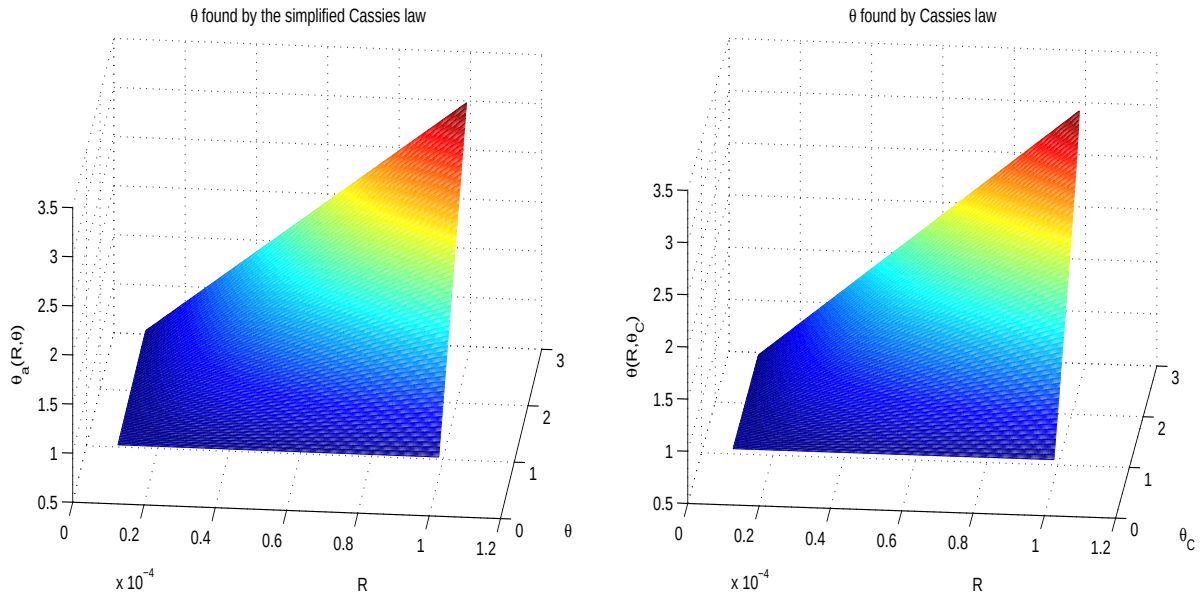

FIGURE 24. To the left $\theta_a(R,\theta)$ with $\theta = \theta_{AC}$ calculated by the simplified Cassie's law (79). To the right $\theta_a(R,\theta)$ with $\theta = \theta_C$ calculated by Cassie's law (76).

Step 1: First, we define $\widetilde{\theta}_a(R, W_I)$ where W_I is a wettability index ranging from 0 (mixed-wet) to 1 (water-wet). Motivated by (22), we suggest to consider the following family of distributions $\widetilde{\theta}_a(R, W_I)$, one for each wetting state represented by W_I.

$$\widetilde{\theta}_a(R, W_I) = a(W_I)R + b(W_I), \tag{84}$$

where

$$a(W_I) = \frac{\theta_{a_{\max}}(W_I) - \theta_{a_{\min}}}{R_{\max} - R_{\min}}, \quad b(W_I) = \theta_{a_{\min}} - \Big(\frac{\theta_{a_{\max}}(W_I) - \theta_{a_{\min}}}{R_{\max} - R_{\min}}\Big) R_{\min}, \tag{85}$$

for $(R, W_I) \in [R_{\min}, R_{\max}] \times [0, 1]$. The following linear relation is used for $\theta_{a_{max}}(W_I)$:

$$\theta_{a_{\max}}(W_I) = cW_I + d, \quad \text{where} \quad c = \frac{\theta_{a_{\min}} - \theta_{a_{\max}}}{W_{I_{\max}} - W_{I_{\min}}}, \quad d = \theta_{a_{\max}}, \tag{86}$$

for $W_I \in [0, 1]$. This ensures that $\theta_{\max}$ decreases as the wetting state W_I goes from a mixed-wet state towards a water-wet state. In Fig. 23 we have shown a plot of $\widetilde{\theta}_a(R, W_I)$. In particular, $\widetilde{\theta}_a(R, W_I)$ has been constructed such that

$$\widetilde{\theta}_a(R, W_I^1) > \widetilde{\theta}_a(R, W_I^2) \quad \forall R \in [R_{\min}, R_{\max}], \qquad \text{when} \qquad W_I^1 < W_I^2. \tag{87}$$

Note that many different choices for the construction of $\widetilde{\theta}_a(R, W_I)$ could have been made. Other distributions could possibly be introduced that describe wettability in a more realistic manner. This remains a topic for further research.

As a first step, however, we have considered a simplest possible choice which is a natural generalization of (22) to a family of different wetting states. The next step is to convert $\widetilde{\theta}_a(R, W_I)$ into a corresponding distribution $\theta_a(R, \theta_C)$ such that θ_C and $\theta_a(R, \theta_C)$ are related by Cassie's law in the sense of (83).

Step 2: For simplicity reasons we first consider the approximated Cassie's law represented by (79). Then in Remark 4.1 we explain why the same construction works for Cassie's law.

Assume that we have distributions $\{W_{I,j}\}_{j=1}^{M}$ and $\{R_i\}_{i=1}^{N}$. Then we define the operator P such that

$$P : W_{I,j} \to \{\widetilde{\theta}_a(R_i, W_{I,j})\}_{i=1}^{N} \to \theta_{AC,j}, \tag{88}$$

where the first mapping is obvious in light of Step 1, whereas the last is defined by the following area average similar to (79):

$$\theta_{AC,j} = \sum_{i=1}^{N} f_i \widetilde{\theta}_a(R_i, W_{I,j}). \tag{89}$$

If we can show that P is one-to-one, i.e.,

$$\theta_{AC,j_1} = \theta_{AC,j_2} \qquad \Rightarrow \qquad W_{I,j_1} = W_{I,j_2}, \tag{90}$$

then P is invertible. Let us check this for P defined by (88) and (89).

Proof. We assume

$$\theta_{AC,j_1} = \theta_{AC,j_2} \tag{91}$$

Then

$$\sum_{i=1}^{N} f_i \widetilde{\theta}_a(R_i, W_{I,j_1}) = \sum_{i=1}^{N} f_i \widetilde{\theta}_a(R_i, W_{I,j_2})$$

or

$$\sum_{i=1}^{N} f_i \Big(\widetilde{\theta}_a(R_i, W_{I,j_1}) - \widetilde{\theta}_a(R_i, W_{I,j_2}) \Big) = 0.$$

Using the fact that $f_i > 0$ for $i = 1, \dots N$, and the fact that either

$$\widetilde{\theta}_a(R_i, W_{I,j_1}) > \widetilde{\theta}_a(R_i, W_{I,j_2}), \qquad \text{for all } i = 1, \dots, N$$

or

$$\widetilde{\theta}_a(R_i, W_{I,j_1}) < \widetilde{\theta}_a(R_i, W_{I,j_2}), \qquad \text{for all } i = 1, \dots, N,$$

which follows from the construction of $\widetilde{\theta}_a(R, W_I)$ as described in Step 1 (see also Fig. 23), we can conclude that

$$\widetilde{\theta}_a(R_i, W_{I,j_1}) = \widetilde{\theta}_a(R_i, W_{I,j_2}), \qquad \text{for all } i = 1, \dots, N.$$

Finally, in view of the monotonicity property described in (87), we can conclude that

$$W_{I,j_1} = W_{I,j_2}.$$

Consequently, the one-to-one property of the operator P as described by (90) has been verified. □

Remark 4.1. *The one-to-one property of P given by* (88) *and* (89) *has been shown. If we replace the approximate Cassie's relation* (89) *by a Cassie's law type of relation*

$$\cos(\theta_{C,j}) = \sum_{i=1}^{N} f_i \cos\widetilde{\theta}_a(R_i, W_{I,j}), \tag{92}$$

the same arguments as above can be repeated since $\cos(x)$ *is strictly monotone in the interval* $[0, \pi]$. *In other words, P is invertible when* (89) *is replaced by* (92).

Consequently, equipped with the family of distributions $\widetilde{\theta}_a(R, W_I)$ from Step 2, we can define the new family $\theta_a(R, \theta_C)$ as follows:

Definition 4.1.

$$\theta_a(R_i, \theta_{C,j}) \stackrel{def}{:=} \widetilde{\theta}_a(R_i, P^{-1}(\theta_{C,j})), \tag{93}$$

for $i = 1, \dots N$ and $j = 1, \dots M$.

Lemma 4.1. *The distribution $\theta_a(R, \theta)$ given by* (93) *has been constructed in such a way that for $\theta^* \in [\theta_{min}, \theta_{max}]$, the corresponding distribution $\theta_a(R, \theta^*)$ satisfies Cassie's law in the sense of* (83).

Proof. Clearly, using that $W_{I,j} = P^{-1}(\theta_{C,j})$ it follows from (92) that

$$\cos(\theta_{C,j}) = \sum_{i=1}^{N} f_i \cos\widetilde{\theta}_a(R_i, W_{I,j}) = \sum_{i=1}^{N} f_i \cos\theta_a(R_i, \theta_{C,j}), \tag{94}$$

where we have used (93). □

Finally, we now want to visualize the constructed $\theta_a(R, \theta_{AC})$ and $\theta_a(R, \theta_C)$ obtained from the procedure described in Step 1 and Step 2. Fig. 24 gives an illustration of the two different functions $\theta_a(R, \theta)$, i.e. first, by letting $\theta = \theta_{AC}$ and then by letting $\theta = \theta_C$, respectively. The figure shows little difference and we therefore choose just to concentrate the further investigation on the last approach, namely by using the Cassie's contact angle as the averaged contact angle θ. We remark that this may not be very surprising in view of the approximation (77) shown in Fig. 22.

4.4. **Assessment of the correlation for Case II.** The purpose now is to make use of the distribution $\theta_a(R, \theta_C)$, which relates the distribution of local contact angles θ_a to Cassie's contact angle θ_C employed in the correlation, to estimate the unknown parameters c_w, a_w, c_o and a_o. This has been done by using the same curve-fitting method as in Section 4.2.

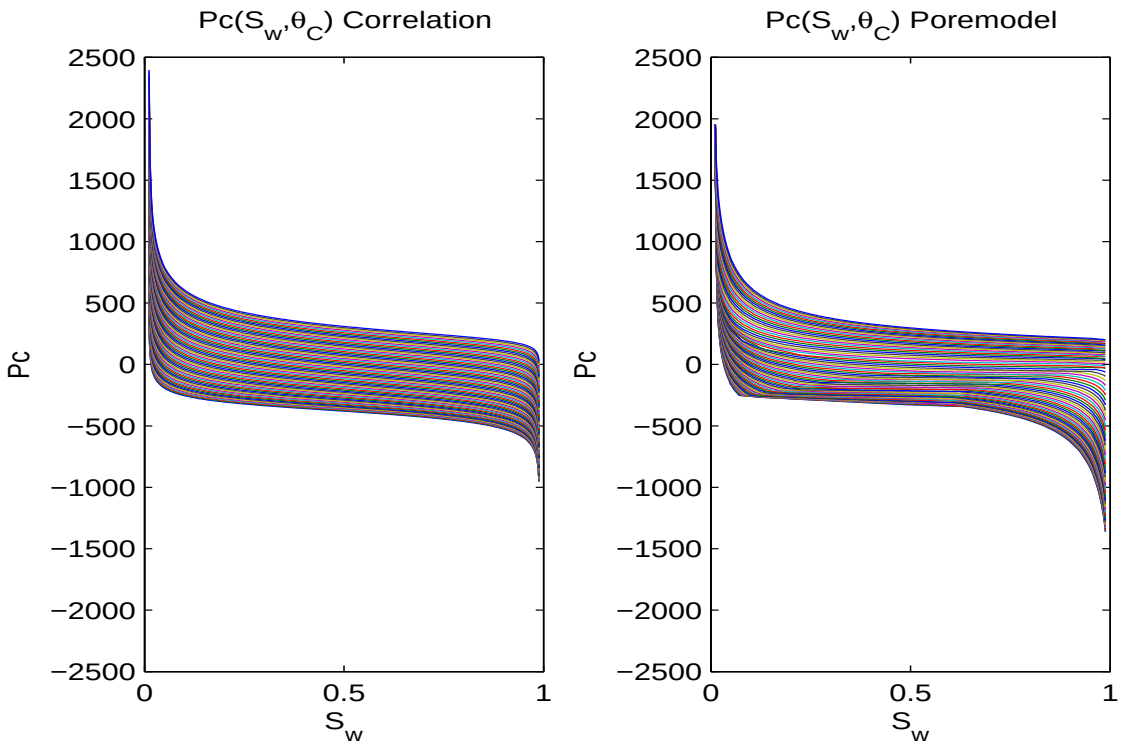

FIGURE 25. **Example 2a): Left:** $Pc^{\mathrm{Corr}}(S_w)$ generated by the correlation (61) with the estimated parameters given by (95). **Right:** The corresponding $Pc^{\mathrm{Pore}}(S_w)$ curves generated by the pore model using (83). In both cases Pc is plotted as a function of S_w for different $\theta_C \in [\theta_{C_{\min}}, \theta_{C_{\max}}]$.

Example 2a). The xdata amounts to the same saturation interval as in Example 1a), with $S_{w,\min} = 0.011$, $S_{w,\max} = 1 - 0.011$, $\triangle S_w = 0.0025$ and $m = 393$. The ydata are now the $M = 71$ different values of $\{\theta_j\}_{j=1}^{M}$ found by Eq. (83) for different sets of local contact angle distributions $\{\theta_a(\cdot, \theta_j)\}_{j=1}^{M}$ defined in (84)–(86) with $\theta_{a_{\max}} = 180°$ and $\theta_{a_{\min}} = 40°$. For these sets of contact angles we have then generated the corresponding values of $Pc(S_w, \theta_C)$ by the pore model giving the zdata. The estimated parameters in this case are given by

$$c_w = 444Pa, \qquad a_w = 0.26, \qquad c_o = 516Pa \qquad \text{and} \qquad a_o = 0.12. \tag{95}$$

Fig. 25 (left) shows a plot of Pc as a function of S_w for the different $\theta_C \in [\theta_{C_{\min}}, \theta_{C_{\max}}]$ generated by the correlation with the estimated parameters (95). To the right are shown the corresponding curves generated by the pore model based on (83). 3D plots of the $Pc^{\mathrm{Corr}}(S_w, \theta_C)$ and $Pc^{\mathrm{Pore}}(S_w, \theta_C)$ curves are shown in Fig. 26. The 3D plots seen from above and a plot of the error $E = |Pc^{\mathrm{Corr}}(S_w, \theta_C) - Pc^{\mathrm{Pore}}(S_w, \theta_C)|$ for this case are shown in Fig. 27 and Fig. 28, respectively.

Observations: In view of Fig. 25 – 28 we may remark:

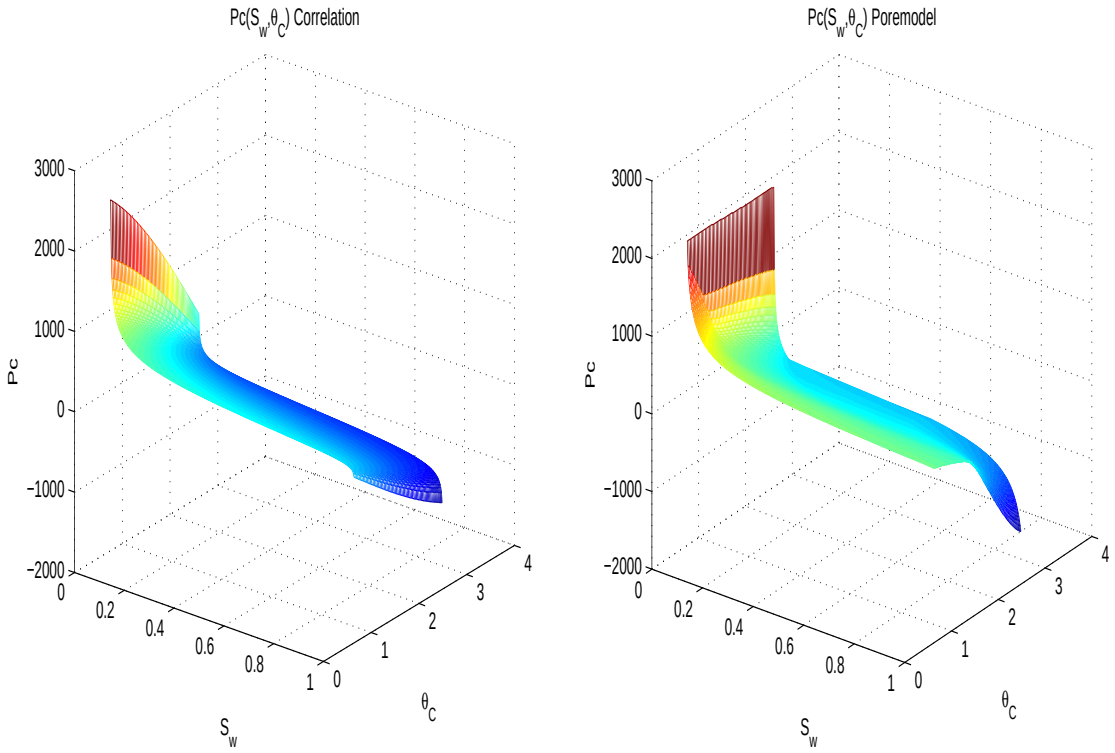

FIGURE 26. **Example 2a): Left:** $Pc^{\mathrm{Corr}}(S_w, \theta_C)$ generated by the correlation (61) with the estimated parameters given by (95). **Right:** The corresponding $Pc^{\mathrm{Pore}}(S_w, \theta_C)$ curves generated by the pore model by using (83).

- Fig. 25 reflects that the correlation gives a fairly good match at the endpoint with low water-saturation. It doesn't capture so well the lowest Pc-values for the highest water-saturations.
- The spreading of the curves generated by the correlation for different θ_C's is similar to that of the pore model, in contrast to Case I, see Fig. 13.
- The error is larger for the high values of θ combined with the smaller water saturation, see Fig. 28. This behavior is also observed in Example 1a), however the absolute value of the error is considerably higher in Example 1a), see Fig. 16.

Example 2b). In this example we have again restricted the saturation area to $S_w \in [0.05, 1-0.05]$ similar to Example 1a). Otherwise, the situation is the same as in Example 2a). The optimization gives the following parameters:

$$c_w = 491Pa, \qquad a_w = 0.18, \qquad c_o = 526Pa \qquad \text{and} \qquad a_o = 0.12. \tag{96}$$

Fig. 29 (left) shows a plot of Pc as a function of S_w for the different $\theta_C \in [\theta_{C_{\min}}, \theta_{C_{\max}}]$ generated by the correlation with the estimated parameters (96). To the right are shown

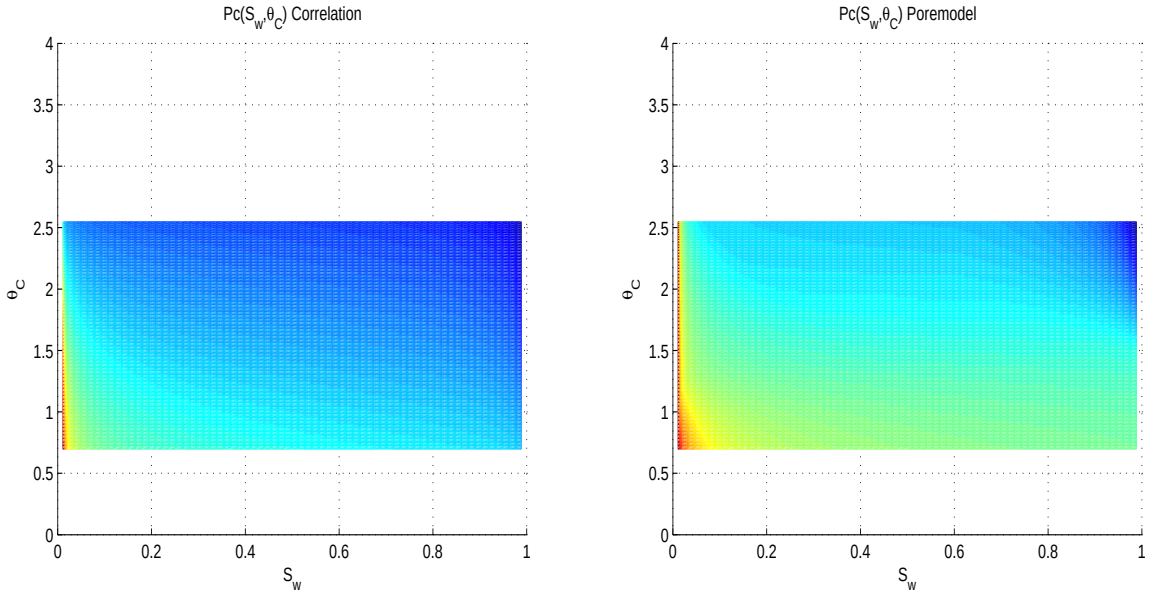

FIGURE 27. **Example 2a):** The curves shown in Fig. 26 seen from above.

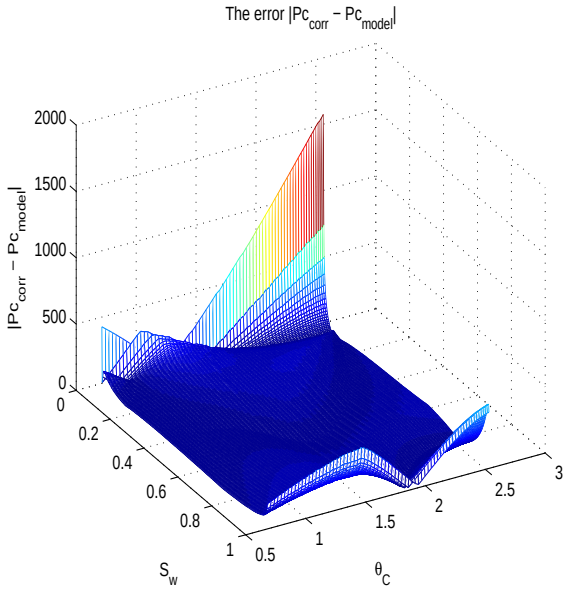

FIGURE 28. **Example 2a):** The error
$E = |Pc^{\mathrm{Corr}}(S_w, \theta_C) - Pc^{\mathrm{Pore}}(S_w, \theta_C)|$ for the curves in Fig. 26.

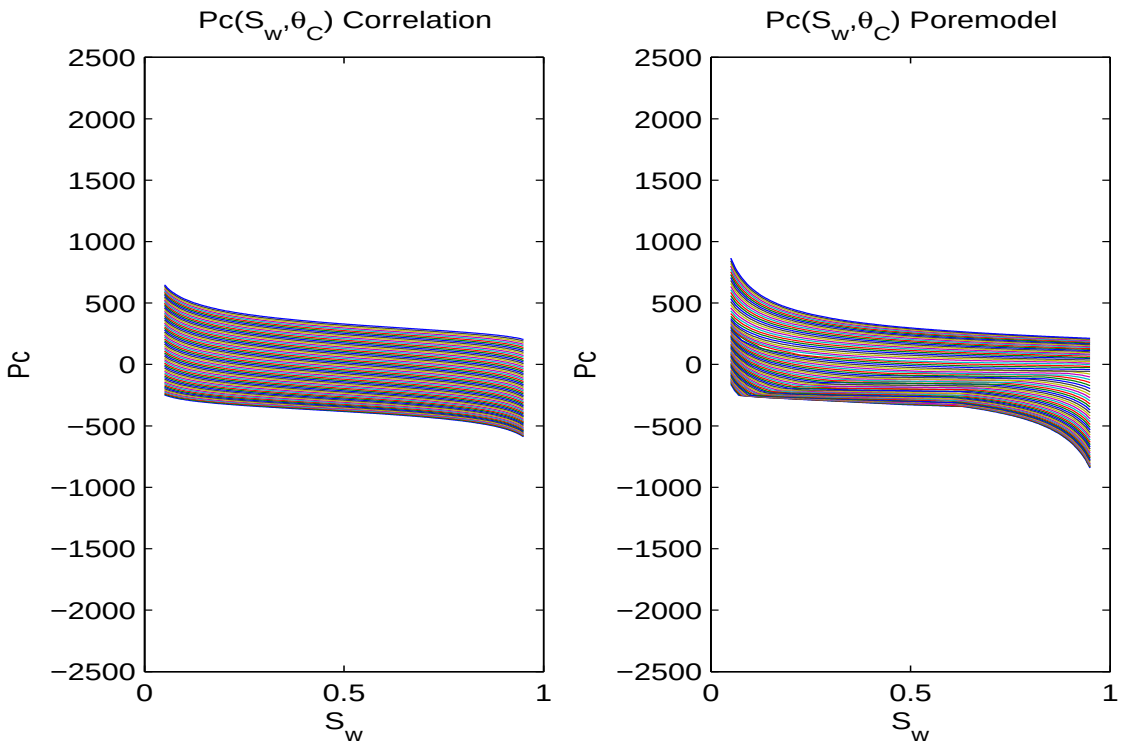

FIGURE 29. **Example 2b):** Plots of the same curves as in Fig. 25 with a reduced saturation interval.

the corresponding curves generated by the pore model based on (83). 3D plots of the $Pc^{\text{Corr}}(S_w, \theta_C)$ and $Pc^{\text{Pore}}(S_w, \theta_C)$ curves are shown in Fig. 30. The 3D plots seen from above and a plot of the error $E = |Pc^{\text{Corr}}(S_w, \theta_C) - Pc^{\text{Pore}}(S_w, \theta_C)|$ are illustrated in Fig. 31 and Fig. 32, respectively.

Observations: In view of Fig. 29 – 32 we may remark:

- The estimated values are changed as follows: c_w and c_o are higher, a_w lowered and a_o remains unchanged.
- Fig. 31 reflects that the correlation captures the main contours much better compared to Case I, see Fig. 19.
- Fig. 32 reflects that the error is highest for the smaller and larger saturation values. However, by comparing with Case I, Example 1b), we see that the absolute error is reduced by a factor of 2, both at the outermost and central parts of the region $(S_w, \theta_C) \in [0.05, 1 - 0.05] \times [\theta_{C_{\min}}, \theta_{C_{\max}}]$.

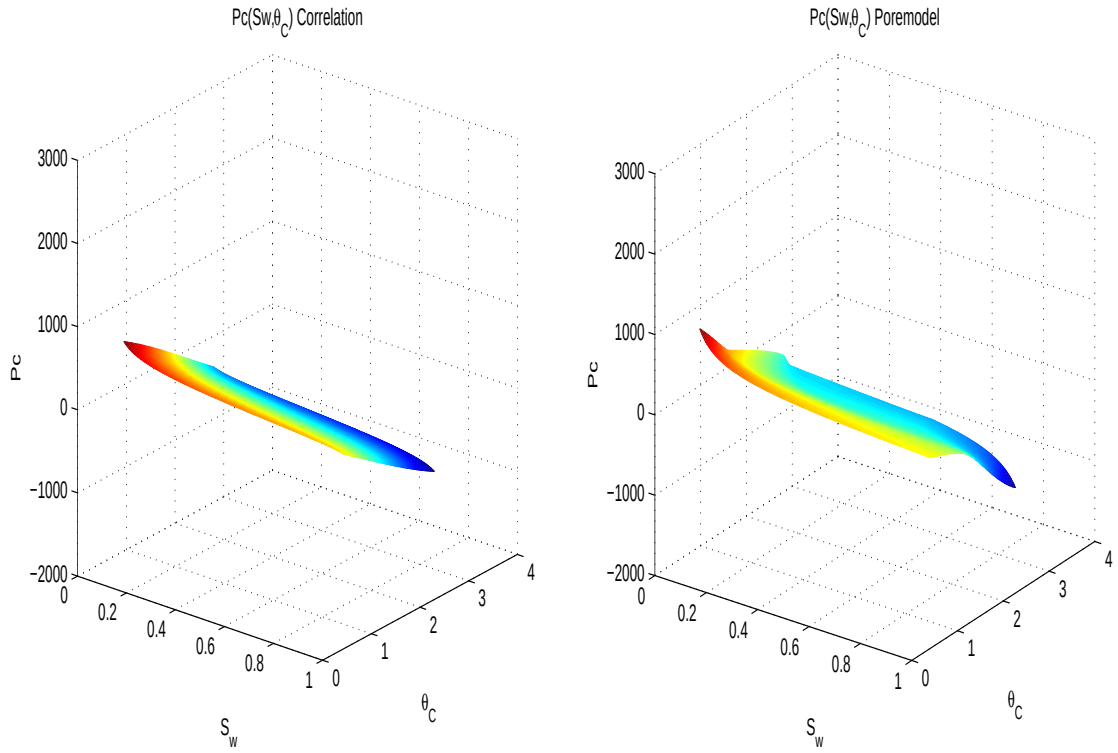

FIGURE 30. **Example 2b):** Plots of the same curves as in Fig. 26 with a reduced saturation interval.

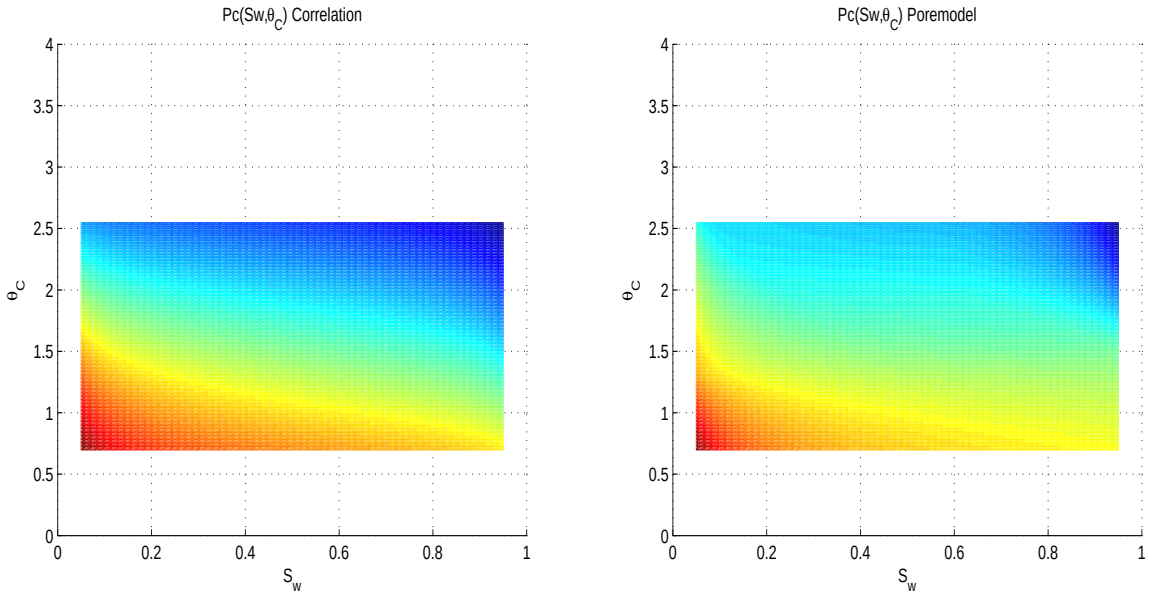

FIGURE 31. **Example 2b):** The curves shown in Fig. 30 seen from above.

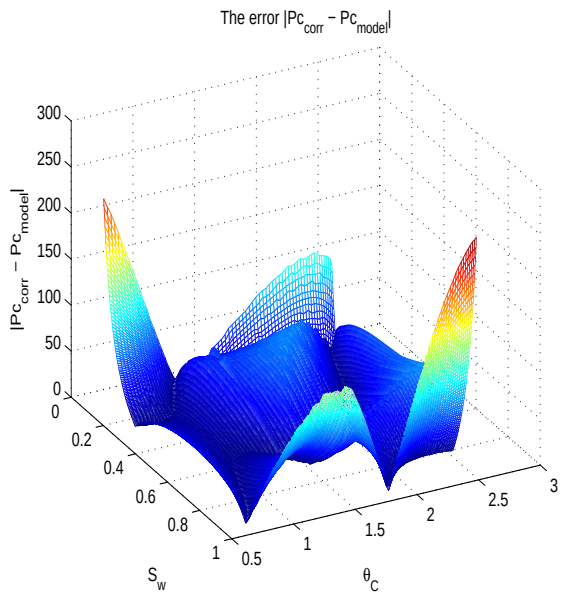

FIGURE 32. **Example 2b):** The error
$E = |Pc^{\mathrm{Corr}}(S_w, \theta_C) - Pc^{\mathrm{Pore}}(S_w, \theta_C)|$ for the curves in Fig. 30.

5. Concluding remarks

Emphasis has been on the development of a framework that allows for systematic investigations of how to design a pore structure whose averaged behavior is captured well by the correlation. As a conclusion, it seems clear that the use of an averaged contact angle based on Cassie's law gives a favorable result in the attempt of representing the pore model by the correlation. In Fig. 33 we have plotted $Pc^{\mathrm{Corr}}(S_w, \theta_C)$ and $Pc^{\mathrm{Pore}}(S_w, \theta_C)$ for different choices of θ_C in the interval $\theta_C \in [\theta_{C_{\min}}, \theta_{C_{\max}}]$. The fit is best for θ_C contained in the central part of the interval. For small θ_C there is a discrepancy for small water saturations S_w. For large θ_C there is a discrepancy for large water saturations S_w. Most likely, this discrepancy could have been reduced by modifying the distribution $\widetilde{\theta}_a(R, W_I)$ given by (84) and (85). More precisely, replace the linear variation with respect to wetting state W_I by a suitable nonlinear variation.

In light of the above comments, some natural further investigations could be as follows:

- One could envision to use a distribution $\widetilde{\theta}_a(R, WI)$ which to a larger extent discern between the two cases $\theta < \pi/2$ (water-wet) and $\theta > \pi/2$ (mixed-wet).
- Furthermore, one could envision to use other distributions for $\widetilde{\theta}_a(R, WI)$ than the linear distribution in R direction and WI direction that have been used, see Fig. 23. Still the framework given by Step 1 and Step 2 in Section 4.3 could serve as a helpful guideline for construction of the corresponding distribution $\theta_a(R, \theta_C)$ which takes into account Cassie's law.

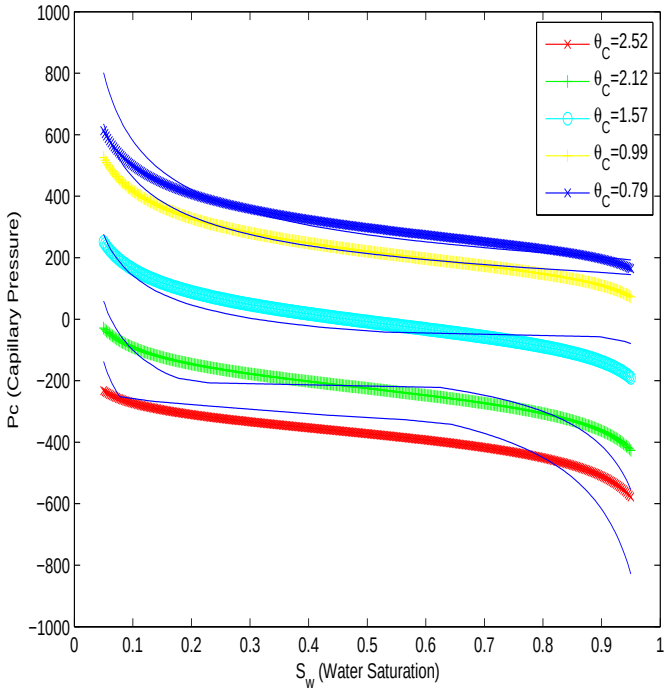

FIGURE 33. Comparison of $Pc^{\text{Corr}}(S_w, \theta_C)$ and $Pc^{\text{Pore}}(S_w, \theta_C)$ for different choices of θ_C.

- The use of Cassie's law is motivated by the desire of taking the heterogeneity of the surface into account. The influence of other factors influencing the local contact angles and hence the wettability of the porous media, as f.ex the roughness of the surface, could also have been considered [10].
- The uniform distribution of the pore sizes is chosen for simplicity. To get a more realistic distribution we could use other distributions as f.ex. Weibull, log-normal or beta-distribution. For the half-angle of the corners α we have chosen a linearly dependency on R. Other choices could have been made.

NOTATION

A	Total area of the cross-section of a tube.
A_w	Area of a tube occupied by water.
A_{ow}	Cross-sectional bulk area bounded by an AM.
AM	Arc meniscus.
α	Half angles of the corners in a pore [rad].
b_{pd}	Length of the pore wall that remains water-wet after primary drainage.
d	Length of the side of a corner in a pore.
L_{sow}	Cross-sectional fluid-solid length.
L_{fow}	Cross-sectional fluid-fluid length.
MTM	Main terminal meniscus.
$N = 300$	Number of pores (tubes) in the model (used here).
$n = 3$	Number of corners in a pore.
o	Oil.
P_c	Capillary pressure (Pa).
$Pc^{max} = 10000$	Capillary pressure at the end of primary drainage.
pd	Primary drainage.
$r = \frac{\sigma}{Pc}$	Radius of curvature.
R	Radii of the inscribed circle for the tubes[m].
$R_{min} = 10^{-6}$	R of the smallest pore[m].
$R_{max} = 100^{-6}$	R of the largest pore[m].
S_w	Water saturation.
S_{wr}	Residual/irreducable water saturation.
S_o	Oil saturation.
S_{or}	Residual/irreducable oil saturation.
$\sigma = 0.020$	The oil-water interfacial tension [N/m].
θ	Effective/averaged contact angle.
θ_a	Advancing contact angle.
θ_{AC}	An approximation of Cassie's contact angle.
θ_C	Cassie's contact angle.
w	Water.
W_I	Wettability index.

Acknowledgement. The author is thankful to the supervisors, prof. Svein M. Skjaeveland at UiS and dr. Johan Olav Helland at IRIS, for introducing me to the theory discussed in this thesis and giving helpful advices. In particular, the matlab code that has been used for the pore model simulations is based on appropriate modifications of the code developed by dr. Helland. A special thank is also given to my husband, Steinar, for counseling and encouragement throughout the work.

References

[1] Clayton T. Crowe. *Multiphase flow handbook*, CRC Press (2006).

[2] M.I.J. van Dijke, K.S.Sorbie Existence of fluid layers in the corners of a capillary with non-uniform wettability. *Journal of Colloid and Interface Science*, 293 (2006) 455 - 463.

[3] S.G.Evje. Some aspects of the Young-Laplace equation for porous media modelling. *Bachelor thesis, University of Stavanger*, June 2008.

[4] S.Evje and J.O.Helland Internal note.

[5] Pierre-Gilles de Gennes, Francoise Brochard-Wyart and David Qur. *Capillarity and Wetting Phenomena*, Springer (2004).

[6] J.O.Helland, M.I.J.van Dijke, K.S.Sorbie, S.M.Skjaeveland Three-phase relative permeability from mixed-wet triangular and star-shaped pores.

[7] J.O.Helland and S.M.Skjaeveland. Physically Based Capillary Pressure Correlation for Mixed-Wet Reservoirs From a Bundle-of-Tubes Model. *SPE Journal*, (June 2006).

[8] Johan Olav Helland Modelling of Three-Phase Capillary Pressure for Mixed-Wet Reservoirs. *Doctor thesis, University of Stavanger*, July 2005.

[9] Masao Iwamatsu The validity of Cassies's law: A simple exercise using a simplified model. *Journal of Colloid and Interface Science*, 294 : 176-181 (2006).

[10] J.Long, M.N.Hyder, R.Y.M.Huang, P.Chen Thermodynamic modeling of contact angles on rough, heterogenous surfaces. *Advances in Colloid and Interface Science*, 118 (2005) 173 - 190.

[11] S.M.Skjaeveland, L.M. Siqveland, A. Kjosavik, Stavanger College, W.L. Hammervold Thomas, Statoil, G.A. Virnovsky, RF-Rogaland Research. Capillary Pressure Correlation for Mixed-Wet Reservoirs. *SPE Reservoir Eval. & Eng. 3(1)*, (February 2000).

[12] Hans Kleppe. Simulation of spontaneous imbibition of seawater into an oil-wet rock. *Internal note/Shell PDO report.*

[13] P.O.Sukka. Improving the Nuclear Tracer Imaging Centrifuge Method for Measuring In-Situ Capillary Pressures and Comparisons with Other Methods. *Doctor thesis, University of Bergen*, December 2004.